

University of Reading
School of Mathematics, Meteorology & Physics

**Examination of non-Time Harmonic Radio Waves
Incident on Plasmas**

by

Andrew Ash

August 2008

This dissertation is submitted to the Department of Mathematics in partial fulfilment of the requirements for the degree of Master of Science

Abstract

The examination of radio waves propagating, interacting and reflecting off various bodies and materials is of interest in many areas of research, including assessing radio communications through the ionosphere, determining effects on soft tissue from mobile phone use and producing radar cross section estimates for military purposes. Analytical solutions exist for only the simplest of geometries where Maxwell's equation can be solved, so to fulfil all of these diverse requirements numerical techniques have been developed, and one such method is the Finite Difference Time Domain (FDTD) approach. This report examines the use of FDTD to model a finite radar pulse on plasma and plasma coated objects, in particular its ability to model the effect of non-time harmonic radar waves. These 'chirped' waves vary in wavelength through the pulse and are utilised by a radar system to negate against countermeasures (such as 'chaff') and to increase the effective power of the pulse. An examination into the number of sampling points of the chirped wave required to produce numerical solutions consistent with electromagnetic theory is presented, along with recommendations for further research.

DECLARATION

I confirm that this is my own work and the use of all material from other sources has been properly and fully acknowledged.

Signed..... (Andrew Ash)

Acknowledgements

I wish to thank Steve Langdon for his assistance and direction while completing this dissertation. I also wish to thank my employer, Defence Science and Technology Laboratory (Dstl) for the financial and managerial support while completing my Masters.

Contents

1. Introduction	1
2. Electromagnetic Theory	5
2.1. Poynting Vector	8
3. Analytic Solutions	9
3.1. Free Space Behaviour	9
3.2. Plane Wave Incident on a PEC Plane	12
3.3. Plane Wave Obliquely Incident on a Dielectric Surface	12
4. Finite Difference Formulation	15
4.1. Yee Grid	16
4.2. Finite Difference Time Domain (FDTD)	19
4.3. Boundary Conditions	22
4.3.1. Mur Boundary Conditions	23
4.4. Incident Wave	24
4.5. Non-time Harmonic Electromagnetic Wave	29
4.6. Truncation Error	30
4.7. Stability	32
4.8. Choice of Grid Spacing	33
5. Plasma Theory	35
5.1. Cold Plasma	37
5.2. Group and Phase Velocity in Plasma	38
6. Numerical Results from Time Harmonic Problem	40
6.1. Plane Wave in Free Space	40
6.2. Plane Wave Incident on a Dielectric Medium	43
6.2.1. Incident Angle = 0 Degrees	43
6.2.2. Incident Angle = 45 Degrees	46
6.3. Conclusions	48
7. Numerical Results from non-Time Harmonic Problem	50
7.1. Incident Wave Representation	51
7.2. Grid Spacing Variation	51
7.3. Variation of Chirp in Incident Wave	56
7.4. Conclusions	61
8. Summary	62
9. References	64
Appendix A: Vector Identities	65

1. Introduction

The generation of radio waves for the purpose of detecting objects at a distance from an observation point, known as Radio Detection and Ranging (RADAR), has been utilised since the early 20th century for both civilian and military purposes. In particular radar has been utilised for detection of aircraft, missiles and other complexly shaped objects. These objects are characterised by a Radar Cross Section (RCS) and a radar signature, determining the overall magnitude of the radar pulses reflected from the object and the variation of this return respectively. The detection range (i.e. the maximum range from a radar dish that an object can be detected) of a particular radar/target pair is determined by the relative magnitude of the returned radar pulse (the 'signal') compared to the ambient background radiation around the radar (the 'noise'); given by the Signal to Noise Ratio (SNR). The radar equation (see [5]) shows that SNR is proportional to the RCS of an object and as such is a key parameter in determining the ability of radar to detect the object.

It has been known from the early invention of radio/radar that the propagation of electromagnetic waves can be affected by the medium which they propagate through. In particular the early experiments using radio waves by Marconi observed that rather than propagate through the Earth's atmosphere into space, radio waves were reflected back towards the Earth. This effect is due to the presence of the ionosphere in the upper atmosphere, which consists of cold, ionised plasma and has an electrical permittivity such that it causes radio wave reflection. As such the effect of plasma on RCS and propagation of radio waves through the ionosphere has been of interest to several areas of research, from radar engineers to the designers of communications systems which utilise radio waves to exchange data with satellites above the ionosphere.

A large amount of work has been performed in the analytical and numerical derivation of RCS and radar signatures of various objects, in particular for military purposes. A comprehensive investigation of analytical RCS values for numerous

basic geometrical shapes is presented in the Radar Cross Section Handbook by Ruck [4]. This also includes methods for obtaining the RCS of complex objects made from superimposing a number of simple shapes together. Additionally analytical solutions for the RCS of non-perfectly conducting materials are discussed, with reference to plasmas and the analytical solution of plasma spheres given by Mie [10]. The book by K. S. Kunz and R. J. Luebbers [1] provides a detailed background in the formulation of numerical methods used to predict RCS and radar signatures of various objects, in particular utilising Finite Difference Time Domain (FDTD). Primarily the examples given for numerically determining the RCS (for example of an F-111 at 5 – 50 MHz with a comparison to measured data) examine the scattered electric field, E^s , derived from a uniform time-harmonic incident field, E^i , across the domain (where the total electric field, E^t is given as the sum of the incident and scattered field, $E^t = E^i + E^s$). The examples in [1, 9] utilise this time-harmonic wave approach to produce numerical solutions for the scattered electric fields, which allow RCS values to be determined. In this report the particular case that will be considered is that of the total electric field solution for a non-time harmonic radar pulse incident on a plasma/dielectric.

In recent years, as computing power has increased significantly, a large amount of work and research has been focussed on the extension and modification of FDTD for RCS determination, many of these papers are found in the Institute of Electrical and Electronics Engineers (IEEE) journals, for instance references [6 - 9]. In the paper by Shalager et al. [6] a number of alternative approaches to the central difference FDTD originally proposed by Yee are compared, with the alternative methods being of higher orders compared to the second order space and time nature of the Yee FDTD scheme. In this report the FDTD approach detailed in [1] is used as this method is well documented in terms of its applicability to the problem of electromagnetic wave propagation.

Research into plasma and its interaction with electromagnetic waves has been ongoing for almost as long as the use of FDTD. The added difficulty when trying to consider real rather than theoretical perfect plasmas is the need to determine the accurate Total Electron Content (TEC) within a region and how it evolves with time. Reference [2] gives some detailed background theory on plasma behaviour. Due to the need of additional numerical (usually Monte-Carlo, Computational Fluid Dynamics (CFD)) computer codes to determine the plasma behaviour, a computer code to determine the RCS of a plasma object is usually de-coupled from the code that will generate the TEC evolution within the region of interest.

From the literature examined in the course of this work, it is apparent that the determination of RCS values for a number of objects is well practised and documented. This has utilised FDTD (in various forms) to examine RCS values at a range of frequencies using time harmonic incident radio waves modelled in the computational domain. The aim of this project is to examine the use of non-time harmonic waves (utilised by a large number of modern, pulse compression radar systems in the form of a 'chirp' pair) to interrogate objects shielded by plasma. In particular, the effect of space steps on the error of the solution in modelling a chirped pulse is examined.

The remainder of this report is structured as follows: -

Section 2 discusses some general electromagnetic theory, in particular the Maxwell equations which govern the propagation of radio waves through a medium.

Section 3 investigates analytical solutions of electromagnetic waves travelling in free space, incident on a Perfectly Electrical Conducting (PEC) surface and obliquely incident on a dielectric medium.

Section 4 formulates the general form of the finite difference equations that are used to produce the numerical solutions for the free space, dielectric and plasma radio wave propagation problems. In this section there are also details of the computational domain (including boundary conditions) and the incident wave that will interrogate the object.

Section 5 describes the nature of plasmas and characterises these regions in terms of their electromagnetic properties.

Section 6 compares the numerical results with analytical solutions for waves in free space and incident on a dielectric surface as detailed in section 3.

Section 7 describes the examination of the effect of plasma on a non-time harmonic electromagnetic wave incident on an object, the most significant problem considered here. A comparison of these results with those expected from electromagnetic/plasma theory is presented.

Section 8 provides a summary of the work covered in this report and presents areas for future research.

2. Electromagnetic Theory

The propagation of electromagnetic waves is governed by four Maxwell equations. These describe the relations between the electric (\underline{E}) and magnetic (\underline{H}) fields and are applicable to electromagnetic wave propagation in both free space and in various media.

Consider a three dimensional problem in which an electromagnetic wave is propagating through free space. Using Cartesian co-ordinates, the electric and magnetic fields can be thought as having individual components in the x, y and z directions. At any single point in the three dimensional domain of the problem, six quantities can be specified, E_x , E_y , E_z , H_x , H_y and H_z , which will describe the total electric and magnetic field in the domain. Here, the subscript denotes which Cartesian direction the component of the electric/magnetic field relates to, and it is noted that these six parameters are scalars. We specify the unit vectors, \underline{i} , \underline{j} and \underline{k} , along the x, y and z Cartesian axes respectively, which allows a vector of each electric and magnetic field to be constructed.

A schematic of the individual electric and magnetic field vector components (at arbitrary points in the domain) is shown in Figure 1.

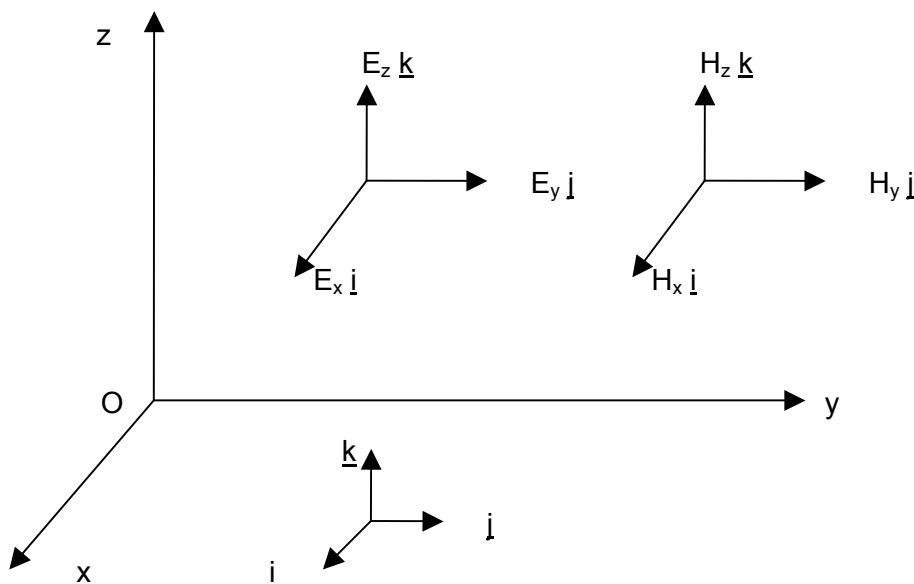


Figure 1: Electric and magnetic fields in Cartesian co-ordinate system

Given these individual electric and magnetic fields, the total field at a point, \underline{r} , in the domain is constructed by the superposition of these components: -

$$\underline{E}(\underline{r}) = E_x \underline{i} + E_y \underline{j} + E_z \underline{k} \quad (1)$$

$$\underline{H}(\underline{r}) = H_x \underline{i} + H_y \underline{j} + H_z \underline{k} \quad . \quad (2)$$

For this project Cartesian co-ordinates will be used throughout.

The four Maxwell equations in Cartesian co-ordinates and differential form are shown in equations (3) to (6): -

$$\nabla \cdot \underline{E} = \frac{\rho}{\epsilon} , \quad (3)$$

$$\nabla \cdot \underline{B} = 0 , \quad (4)$$

$$\nabla \times \underline{E} = -\frac{\partial \underline{B}}{\partial t} , \quad (5)$$

$$\nabla \times \underline{B} = \mu \underline{J} + \mu \epsilon \frac{\partial \underline{E}}{\partial t} , \quad (6)$$

where,

$\underline{J} = \sigma \underline{E}$ is the displacement current (Am^{-2}).

$\underline{B} = \mu \underline{H}$ is the magnetic field density (Wm^{-2}).

\underline{E} is the electric field (Vm^{-1}).

\underline{H} is the magnetic field (Am^{-1}).

ϵ is the electric permittivity (Fm^{-1}) and is expressed in terms of the relative permittivity ϵ_r , compared to free space, ϵ_0 , $\epsilon = \epsilon_r \epsilon_0$.

μ is the magnetic permeability (Hm^{-1}).

ρ represents the charge density (electrons per m^3).

σ is the conductivity of the medium ($\Omega^{-1}\text{m}^{-1}$).

Equations (3) and (4) are contained within (5) and (6), which can be shown by considering the divergence of each. Firstly, we take the divergence of equation (5): -

$$\nabla \cdot \nabla \times \underline{E} = \nabla \cdot \frac{-\partial \underline{B}}{\partial t} . \quad (7)$$

The divergence of a curl of a vector field is zero; this is shown in Appendix A, Lemma 1, so we use the identity: -

$$\nabla \cdot \nabla \times \underline{E} = 0 , \quad (8)$$

Therefore, returning to (7) we see that we have: -

$$0 = -\frac{\partial}{\partial t} \nabla \cdot \underline{B} . \quad (9)$$

This implies that the divergence of the magnetic field \underline{B} is constant with time. Without loss of generality we set \underline{B} to be zero at $t = 0$, and hence this implies that the divergence of \underline{B} is zero at all times.

Similarly, taking the divergence of (6) and again using Appendix A, Lemma 1: -

$$\nabla \cdot (\nabla \times \underline{B}) = \mu \nabla \cdot \underline{J} + \mu \varepsilon \nabla \cdot \left(\frac{\partial \underline{E}}{\partial t} \right) , \quad (10)$$

$$\Rightarrow 0 = \nabla \cdot \underline{J} + \varepsilon \frac{\partial}{\partial t} \nabla \cdot \underline{E} , \quad (11)$$

$$\Rightarrow \varepsilon \frac{\partial}{\partial t} (\nabla \cdot \underline{E}) = -\nabla \cdot \underline{J} . \quad (12)$$

Now, we use the continuity equation (from standard electromagnetic theory, see [3]), which describes the displacement current, \underline{J} , in terms of the change in electron density, ρ :-

$$\nabla \cdot \underline{J} = -\frac{\partial \rho}{\partial t}, \quad (13)$$

which when substituted into (12) gives: -

$$\frac{\partial}{\partial t}(\epsilon \nabla \cdot \underline{E}) = \frac{\partial}{\partial t}(\rho), \quad (14)$$

$$\Rightarrow \nabla \cdot \underline{E} = \frac{\rho}{\epsilon} + C, \quad (15)$$

and we can set the constant to be zero at zero time without loss of generality, which gives Maxwell's equation as expressed in equation (3).

2.1. Poynting Vector

The Poynting vector, denoted by the vector \underline{S} , describes the direction of energy flow of an electromagnetic wave. In simplistic terms, this gives the direction of propagation of the electromagnetic wave, and is given mathematically by [3]: -

$$\begin{aligned} \underline{S} = \underline{E} \times \underline{H} &= \begin{vmatrix} \underline{i} & \underline{j} & \underline{k} \\ E_x & E_y & E_z \\ H_x & H_y & H_z \end{vmatrix}, \quad (16) \\ &= \underline{i}(E_y H_z - E_z H_y) - \underline{j}(E_x H_z - E_z H_x) + \underline{k}(E_x H_y - E_y H_x) \end{aligned}$$

this identity can be used to investigate the direction of propagation of the initial wave and of the scattered fields from the numerical solution.

3. Analytical Solutions

3.1. Free Space Behaviour

For all the problems being modelled in this project, a radar pulse will initially travel in free space (that is a region which has no free electric currents and a permittivity equal to that of free space permittivity, which can therefore be described as lossless) towards a target, and the scattered field from the target will propagate away in free space. Therefore it is necessary to categorise the incident radar pulse in terms of electric and magnetic field distributions at zero time. The mathematical formulation of this can be found by considering Maxwell's equations (5) and (6) in free space, i.e. where $\rho = 0$, $\varepsilon = \varepsilon_0$, $\mu = \mu_0$, $\sigma = 0$ and hence $\underline{J} = 0$: -

$$\nabla \times \underline{E} = \mu_0 \frac{-\partial \underline{H}}{\partial t}, \quad (17)$$

$$\nabla \times \underline{H} = \varepsilon_0 \frac{\partial \underline{E}}{\partial t}. \quad (18)$$

We can now apply the curl operator to both of these expressions: -

$$\nabla \times (\nabla \times \underline{E}) = \nabla \times \left(\mu_0 \frac{-\partial \underline{H}}{\partial t} \right), \quad (19)$$

$$\Rightarrow \nabla(\nabla \cdot \underline{E}) - \nabla^2 \underline{E} = \mu_0 \frac{-\partial}{\partial t} (\nabla \times \underline{H}). \quad (20)$$

Here, we have used the expression for curl of the curl of a vector field, which is found in Appendix A, Lemma 2. Now using the expression for curl \underline{H} from (18), and for divergence of \underline{E} from (3): -

$$\Rightarrow \nabla \left(\frac{\rho}{\varepsilon_0} \right) - \nabla^2 \underline{E} = \mu_0 \frac{-\partial}{\partial t} \left(\varepsilon_0 \frac{\partial \underline{E}}{\partial t} \right), \quad (21)$$

$$\Rightarrow \nabla^2 \underline{E} = \mu_0 \varepsilon_0 \frac{\partial^2 \underline{E}}{\partial t^2}, \quad (22)$$

since the free space charge density, ρ , is zero as mentioned above. The equation (22) is of the form of a generic equation for a wave. Similarly it can be derived that for the magnetic field: -

$$\nabla^2 \underline{H} = \mu_0 \varepsilon_0 \frac{\partial^2 \underline{H}}{\partial t^2}. \quad (23)$$

So both the electric fields and magnetic fields will act as waves when travelling in free space, with the phase velocity, c , given by $(\mu_0 \varepsilon_0)^{-1/2}$.

A radar system such as a phased array radar (see [5] for details) produces plane waves, that is the electric and magnetic fields are constant within a plane at an instant in time. In the case of a phased array radar, a number of dipoles are arranged within the face which can produce an electric field between them varying with time. These are excited by an electrical signal which is sinusoidal in nature, thus alternating the electric field between the dipoles in the same manner. As the electric fields alternate they are radiated out into space, producing a sinusoidal wave in both electric and associated magnetic field.

Without loss of generality, the equation of a plane wave can be expressed as in (24), where z corresponds to the z axis as defined in Figure 1: -

$$\underline{E} = \underline{E}_0 \exp[i(\omega t - kz)], \quad (24)$$

the imaginary part of \underline{E}_0 contains information on the initial phase of the wave.

Taking the real part of this expression gives: -

$$\underline{E} = \underline{E}_0 \cos(\kappa + \omega t - kz), \quad (25)$$

where κ is the phase of the wave. In expressions (24) and (25), k denotes the wavenumber of the plane wave ($=2\pi/\lambda$), ωt gives the temporal evolution of the wave, where ω represents the frequency of the wave (in radians per second),

and t is the time in seconds. From standard wave theory, $c=f\lambda$, where f is the frequency and λ is the wavelength of the electromagnetic wave.

The associated magnetic field is given by: -

$$\underline{H} = \underline{H}_0 \cos(\kappa + \omega t - kz), \quad (26)$$

i.e. the magnetic fields are in phase with the electric fields, and have the same wavenumber (and therefore the same wavelength and frequency). Figure 2 shows the arrangement of electric and magnetic fields in the plane wave.

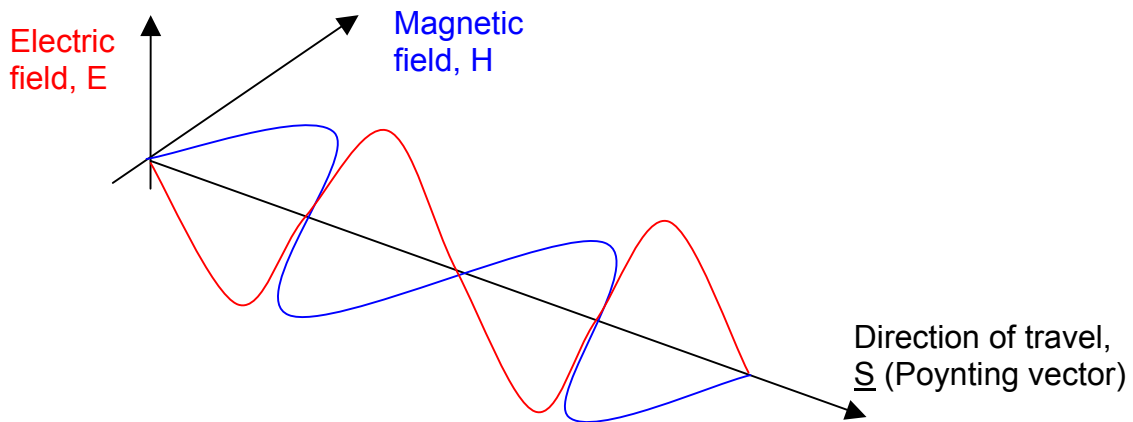


Figure 2: Electric and magnetic fields in incident radar wave. Note that the magnetic field is in the H-S plane and the electric field is in the E-S plane

The phase velocity, v_p , of the plane wave can be determined from the wavenumber and frequency of the wave [3]: -

$$v_p = \frac{\omega}{k} \equiv \frac{f}{\lambda} = c. \quad (27)$$

Therefore a electromagnetic plane wave in free space will propagate in straight lines at a speed that is equivalent to the speed of light in free space, c , which has the value [3]: -

$$c = 299792458 \times 10^8 \text{ ms}^{-1}.$$

3.2. Plane Wave Incident on a PEC Plane

When examining the scattering of an electromagnetic wave off a solid object, it is often assumed that the target being interrogated is made of Perfectly Electrical Conductor (PEC). Essentially this means that the target comprises of a material that is close to a perfect conductor, such that electromagnetic waves incident on the target are reflected away with no appreciable degradation in amplitude of the incident wave. Explicitly, PEC can be characterized as follows: -

Electrical Permittivity, $\epsilon_r \rightarrow \infty$.

Many metals commonly used in the construction of airframes, such as aluminium and titanium, have extremely high electrical permittivities for a large range of frequencies incident upon them, and as such may be approximated by PEC.

3.3 Plane Wave Obliquely Incident on a Dielectric Surface

We consider an electromagnetic plane wave incident on a dielectric material at an angle ζ_i to the normal of the surface. The effect of having a dielectric material rather than a PEC surface is that its electrical permittivity is of a similar order of magnitude compared to the permittivity of free space, ϵ_0 , with a relative permittivity, ϵ_r , greater than one. Figure 3 shows this arrangement, where we have the electric field, E_x , perpendicular to the surface that it is incident upon. The superscript i denotes the incident wave electric and magnetic fields, t denotes the transmitted wave and r denotes the reflected wave: -

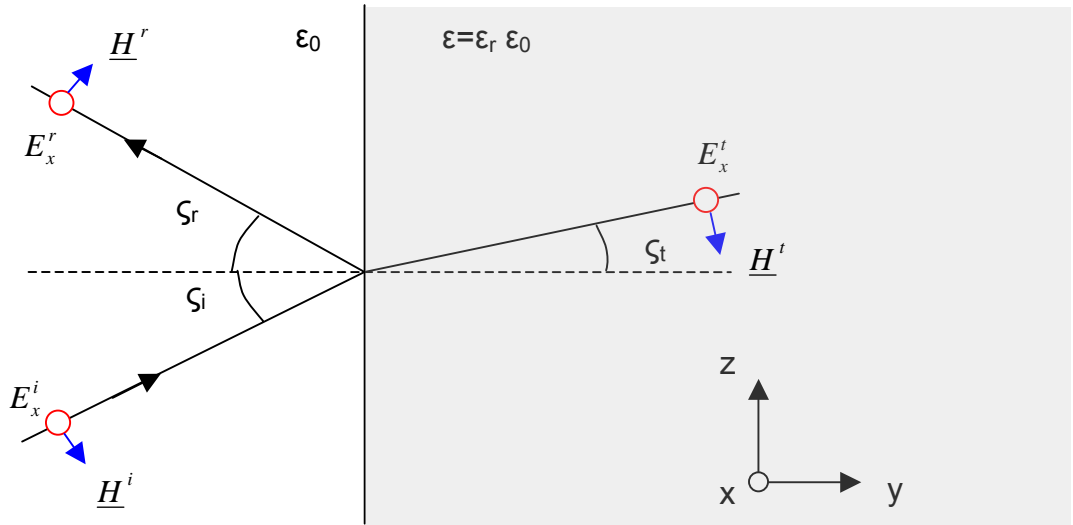


Figure 3: Plane wave obliquely incident on a dielectric

Standard theory from electromagnetics [3] is used to solve this situation to give expressions for the magnitude of the transmitted and reflected electric field component of the electromagnetic wave and the direction of travel relative to the normal of the material (ζ_t). These are known as the perpendicular Fresnel equations ((28) and (29)) and Snell's laws ((30) and (31)) respectively [3]: -

$$|E_x^r| = |E_x^i| \frac{(\sqrt{\epsilon_r} \cos \zeta_t)^{-1} - (\cos \zeta_i)^{-1}}{(\sqrt{\epsilon_r} \cos \zeta_t)^{-1} + (\cos \zeta_i)^{-1}} \quad , \quad (28)$$

$$|E_x^t| = |E_x^i| \frac{2(\sqrt{\epsilon_r} \cos \zeta_t)^{-1}}{(\sqrt{\epsilon_r} \cos \zeta_t)^{-1} + (\cos \zeta_i)^{-1}} \quad , \quad (29)$$

$$\zeta_i = \zeta_r \quad , \quad (30)$$

$$\sin \zeta_t = \frac{\sin \zeta_i}{\sqrt{\epsilon_r}} \quad . \quad (31)$$

For a homogenous medium, defined by the relative permittivity ϵ_r , we can also get an expression for the change in wavelength that will be associated with this transition from free space to the medium. If the incident wave is characterized by

wave number $k_i = 2\pi/\lambda_i$, and the transmitted wave by $k_t = 2\pi/\lambda_t$ (λ_i and λ_t are the wavelengths of the incident and transmitted waves respectively), then: -

$$k_t = k_i \frac{\sin \zeta_i}{\sin \zeta_t} = k_i \sqrt{\epsilon_r} \quad , \quad (32)$$

$$\Rightarrow \lambda_t = \frac{\lambda_i}{\sqrt{\epsilon_r}} \quad . \quad (33)$$

In moving from free space to a dielectric medium, (with $\epsilon_r > 1$ by definition), we see that there will be a reduction in wavelength of the incident wave.

4. Finite Difference Formulation

Finite differences are commonly used in numerical methods to approximate differentials in terms of gradients calculated from closely spaced points on the function. Generally for first order partial differential we use the approximation: -

$$\frac{\partial f(a)}{\partial x} \approx \frac{f\left(a + \frac{\Delta x}{2}\right) - f\left(a - \frac{\Delta x}{2}\right)}{\Delta x} . \quad (34)$$

To use finite differences for electromagnetics, consider the Maxwell equation (3) which gives a temporal variation of electric field, \underline{E} , in terms of a spatial variation of magnetic field, \underline{H} . We can use the definition of the curl operator to give expressions for the rate of change of the electric field in the x, y and z components: -

$$\epsilon \frac{\partial \underline{E}}{\partial t} = \nabla \times \underline{H} - \sigma \underline{E} , \quad (35)$$

$$\Rightarrow \epsilon \frac{\partial \underline{E}}{\partial t} = \begin{vmatrix} \underline{i} & \underline{j} & \underline{k} \\ \frac{\partial}{\partial x} & \frac{\partial}{\partial y} & \frac{\partial}{\partial z} \\ H_x & H_y & H_z \end{vmatrix} - \sigma \underline{E} . \quad (36)$$

By equating terms in the same unit vector directions, \underline{i} , \underline{j} and \underline{k} , we produce three equations representing the x, y and z components of the electric field: -

$$\epsilon \frac{\partial E_x}{\partial t} = \left[\frac{\partial H_z}{\partial y} - \frac{\partial H_y}{\partial z} \right] - \sigma E_x , \quad (37)$$

$$\epsilon \frac{\partial E_y}{\partial t} = \left[\frac{\partial H_x}{\partial z} - \frac{\partial H_z}{\partial x} \right] - \sigma E_y , \quad (38)$$

$$\epsilon \frac{\partial E_z}{\partial t} = \left[\frac{\partial H_y}{\partial x} - \frac{\partial H_x}{\partial y} \right] - \sigma E_z . \quad (39)$$

We can also use this method to produce equations for the magnetic field in the x, y and z components.

$$\mu \frac{-\partial \underline{H}}{\partial t} = \begin{bmatrix} \underline{i} & \underline{j} & \underline{k} \\ \frac{\partial}{\partial x} & \frac{\partial}{\partial y} & \frac{\partial}{\partial z} \\ E_x & E_y & E_z \end{bmatrix} - \sigma^* \underline{H}, \quad (40)$$

Here, we have modified equation (3) to include a magnetic loss term (σ^*H terms, where σ^* is the magnetic conductivity), which is analogous to the electric loss term represented by $\sigma \underline{E}$ in equation (36). These terms allow the possibility of the region in which the electromagnetic waves propagate to induce a magnetic loss. Equating terms in the \underline{i} , \underline{j} and \underline{k} directions we obtain equations (41) to (43): -

$$\mu \frac{-\partial H_x}{\partial t} = \left[\frac{\partial E_z}{\partial y} - \frac{\partial E_y}{\partial z} \right] - \sigma^* H_x, \quad (41)$$

$$\mu \frac{-\partial H_y}{\partial t} = \left[\frac{\partial E_x}{\partial z} - \frac{\partial E_z}{\partial x} \right] - \sigma^* H_y, \quad (42)$$

$$\mu \frac{-\partial H_z}{\partial t} = \left[\frac{\partial E_y}{\partial x} - \frac{\partial E_x}{\partial y} \right] - \sigma^* H_z. \quad (43)$$

In this project we will only be considered lossy dielectric materials, and therefore we shall discount the magnetic conductivity terms.

4.1. Yee Grid

The Yee grid was proposed in Yee's paper of 1966 [13] and allows a problem featuring electromagnetics to be modelled using a finite differences approach. The grid has interleaved electric and magnetic fields along with points that are null (having no electric or magnetic field). Firstly the computational domain, a grid of size $L_x L_y L_z$, is discretised in the x, y and z directions, with rectangular cells of

size $\Delta x \Delta y \Delta z$, where Δx , Δy and Δz are the grid spacings in the x, y and z directions respectively. The grid points within the domain are represented by the vectors \underline{r} , whose position is represented by the indices (m, p, q): -

$$\underline{r} = (m\Delta x)\underline{i} + (p\Delta y)\underline{j} + (q\Delta z)\underline{k}, \quad (44)$$

where,

$$m = 1, 2, \dots, M \quad p = 1, 2, \dots, P \quad q = 1, 2, \dots, Q$$

and,

$$\Delta x = \frac{L_x}{M} \quad \Delta y = \frac{L_y}{P} \quad \Delta z = \frac{L_z}{Q}$$

A schematic of the computational grid is shown in Figure 4: -

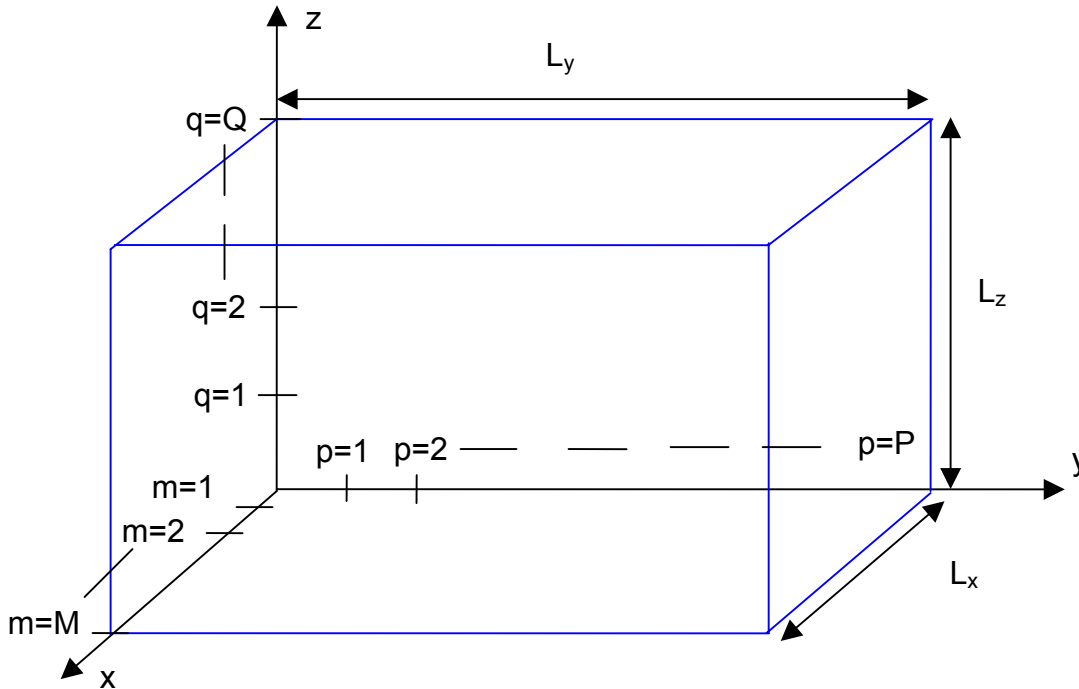


Figure 4: Computational domain

The electric fields and magnetic fields are both represented on a grid with spacings Δx , Δy and Δz . Each Yee cell has face centred electric/magnetic fields as shown in Figure 5: -

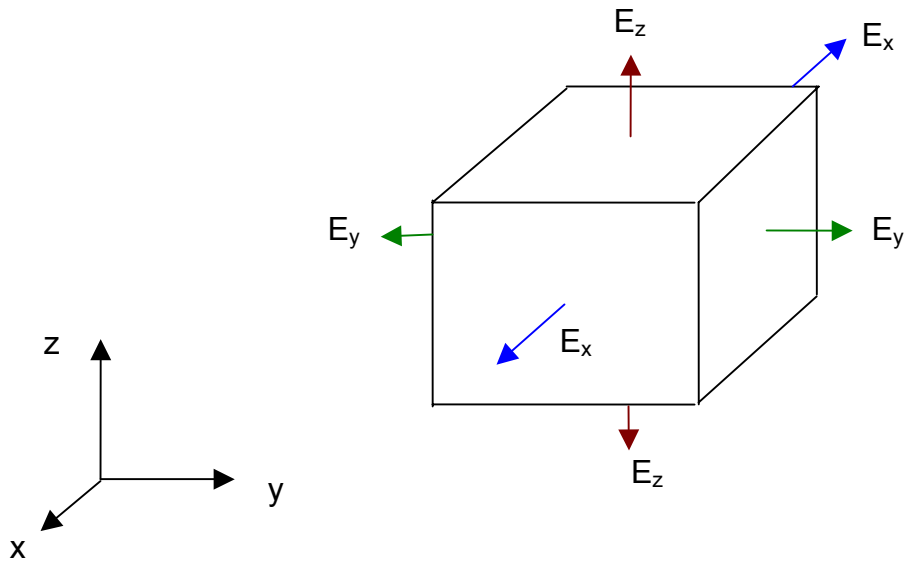


Figure 5: Yee Grid cell for electric fields

However, the magnetic field grid is displaced by a distance: -

$$\frac{\Delta x}{2} \underline{i} + \frac{\Delta y}{2} \underline{j} + \frac{\Delta z}{2} \underline{k}, \quad (45)$$

from the electric field grid. A representation of the Yee grid is shown below in Figure 6: -

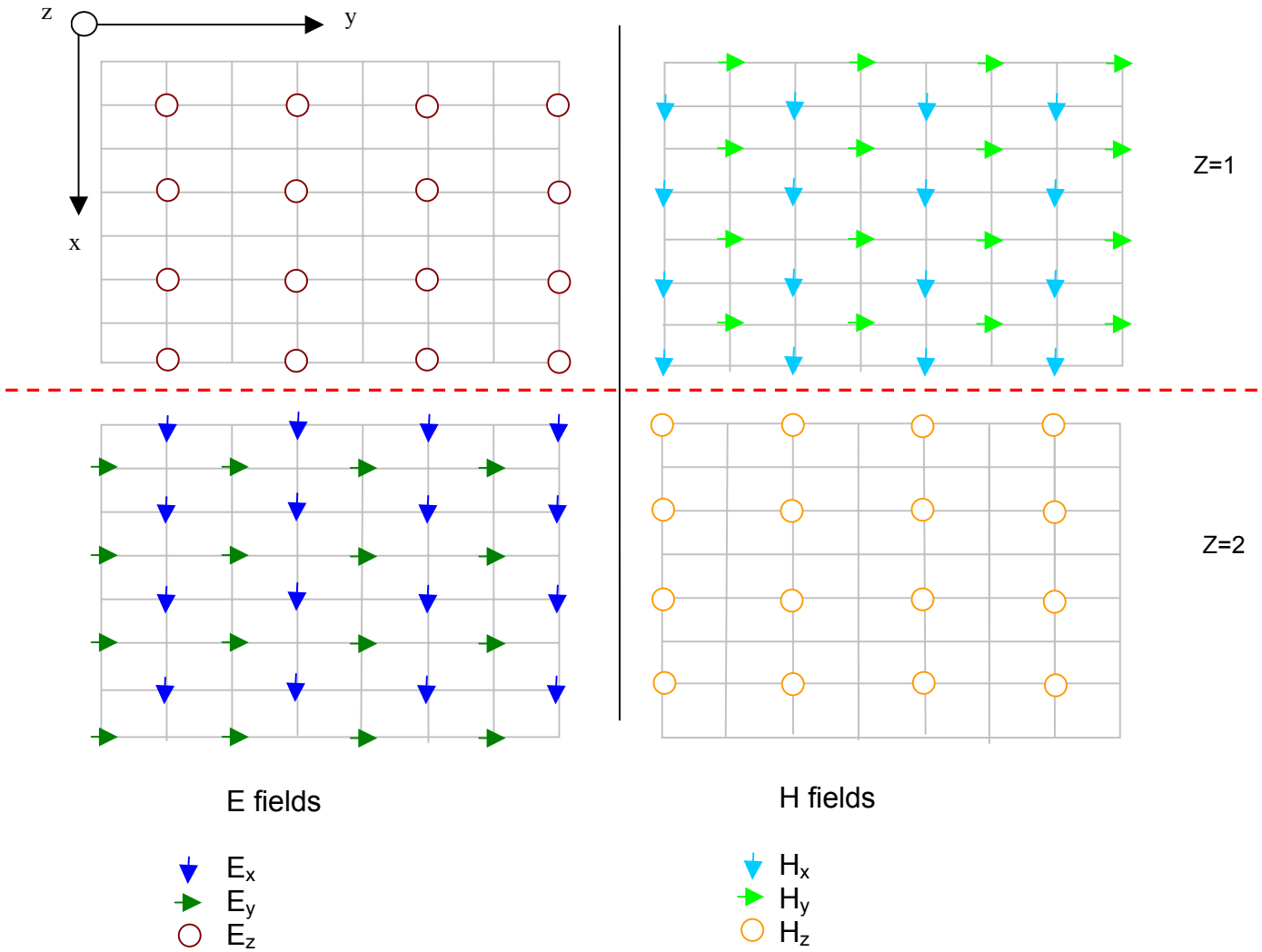


Figure 6: Yee Grid arrangement of electric and magnetic fields

It can be seen from this figure that electric fields circulate around a perpendicular magnetic field and vice-versa. Therefore this grid design complies with Maxwell's equations on a fundamental level, as this effect is observed physically.

4.2. Finite Difference Time Domain (FDTD)

To model electromagnetic wave propagation on a computer we must discretise the computational region (defined in section 4.1.) and to do this we use central

differences to approximate the six equations (37) to (39) and (41) to (43) which describe electromagnetic propagation in 3 dimensions: -

$$\mu \left[\frac{H_x|_{m,p,q}^{n+1} - H_x|_{m,p,q}^n}{\Delta t} \right] = \left[\frac{E_y|_{m,p,q+1}^{n+\frac{1}{2}} - E_y|_{m,p,q}^{n+\frac{1}{2}}}{\Delta z} \right] - \left[\frac{E_z|_{m,p+1,q}^{n+\frac{1}{2}} - E_z|_{m,p,q}^{n+\frac{1}{2}}}{\Delta y} \right] \quad (46)$$

$$\mu \left[\frac{H_y|_{m,p,q}^{n+1} - H_y|_{m,p,q}^n}{\Delta t} \right] = \left[\frac{E_z|_{m+1,p,q}^{n+\frac{1}{2}} - E_z|_{m,p,q}^{n+\frac{1}{2}}}{\Delta x} \right] - \left[\frac{E_x|_{m,p,q+1}^{n+\frac{1}{2}} - E_x|_{m,p,q}^{n+\frac{1}{2}}}{\Delta z} \right] \quad (47)$$

$$\mu \left[\frac{H_z|_{m,p,q}^{n+1} - H_z|_{m,p,q}^n}{\Delta t} \right] = \left[\frac{E_x|_{m,p+1,q}^{n+\frac{1}{2}} - E_x|_{m,p,q}^{n+\frac{1}{2}}}{\Delta y} \right] - \left[\frac{E_y|_{m+1,p,q}^{n+\frac{1}{2}} - E_y|_{m,p,q}^{n+\frac{1}{2}}}{\Delta x} \right] \quad (48)$$

$$\varepsilon \left[\frac{E_x|_{m,p,q}^{n+1} - E_x|_{m,p,q}^n}{\Delta t} \right] = \left[\frac{H_z|_{m,p+1,q}^{n+\frac{1}{2}} - H_z|_{m,p,q}^{n+\frac{1}{2}}}{\Delta y} \right] - \left[\frac{H_y|_{m,p,q+1}^{n+\frac{1}{2}} - H_y|_{m,p,q}^{n+\frac{1}{2}}}{\Delta z} \right] - \sigma E_x \quad (49)$$

$$\varepsilon \left[\frac{E_y|_{m,p,q}^{n+1} - E_y|_{m,p,q}^n}{\Delta t} \right] = \left[\frac{H_x|_{m,p,q+1}^{n+\frac{1}{2}} - H_x|_{m,p,q}^{n+\frac{1}{2}}}{\Delta z} \right] - \left[\frac{H_z|_{m+1,p,q}^{n+\frac{1}{2}} - H_z|_{m,p,q}^{n+\frac{1}{2}}}{\Delta x} \right] - \sigma E_y \quad (50)$$

$$\varepsilon \left[\frac{E_z|_{m,p,q}^{n+1} - E_z|_{m,p,q}^n}{\Delta t} \right] = \left[\frac{H_y|_{m+1,p,q}^{n+\frac{1}{2}} - H_y|_{m,p,q}^{n+\frac{1}{2}}}{\Delta x} \right] - \left[\frac{H_x|_{m,p+1,q}^{n+\frac{1}{2}} - H_x|_{m,p,q}^{n+\frac{1}{2}}}{\Delta y} \right] - \sigma E_z \quad (51)$$

The n+1/2 timesteps seen in these equations allude to the ‘leap-frog’ approach of the FDTD method. This problem is an example of an Initial Value Problem and hence we assign an electric/magnetic field distribution within the computational grid, then progress time forward to see the evolution of the individual fields within the domain, so that a scattered field can be found. The initial electric fields are set up to represent a radar pulse as described in section 4.4., these represent the initial n=0 E-fields, and n=1/2 H-fields. On the first loop of the code, the electric

fields within the bulk of the computational domain are calculated, using explicit expressions for the $n=1$ E-fields (52) to (54) based on the $n=1/2$ H-fields. After all these have been determined, the magnetic fields within the bulk of the domain are determined for the $n=3/2$ time step using the newly calculated $n=1$ E-fields (equations (55) to (57)). This process is repeated at each time step to get from the n to $n+1$, producing a leap-frog method in which E-fields are determined using the $n+1/2$ H-fields, and the H-fields from the n E-fields; as described by equations (52) to (57).

$$E_x \Big|_{m,p,q}^{n+1} = \frac{\left[E_x \Big|_{m,p,q}^n + \frac{\Delta t}{\varepsilon} \left(\frac{H_z \Big|_{m,p+1,q}^{n+\frac{1}{2}} - H_z \Big|_{m,p,q}^{n+\frac{1}{2}}}{\Delta y} - \frac{H_y \Big|_{m,p,q+1}^{n+\frac{1}{2}} - H_y \Big|_{m,p,q}^{n+\frac{1}{2}}}{\Delta z} \right) \right]}{\left(1 + \frac{\Delta t \sigma}{\varepsilon} \right)} \quad (52)$$

$$E_y \Big|_{m,p,q}^{n+1} = \frac{\left[E_y \Big|_{m,p,q}^n + \frac{\Delta t}{\varepsilon} \left(\frac{H_x \Big|_{m,p,q+1}^{n+\frac{1}{2}} - H_x \Big|_{m,p,q}^{n+\frac{1}{2}}}{\Delta z} - \frac{H_z \Big|_{m+1,p,q}^{n+\frac{1}{2}} - H_z \Big|_{m,p,q}^{n+\frac{1}{2}}}{\Delta x} \right) \right]}{\left(1 + \frac{\Delta t \sigma}{\varepsilon} \right)} \quad (53)$$

$$E_z \Big|_{m,p,q}^{n+1} = \frac{\left[E_z \Big|_{m,p,q}^n + \frac{\Delta t}{\varepsilon} \left(\frac{H_y \Big|_{m+1,p,q}^{n+\frac{1}{2}} - H_y \Big|_{m,p,q}^{n+\frac{1}{2}}}{\Delta x} - \frac{H_x \Big|_{m,p+1,q}^{n+\frac{1}{2}} - H_x \Big|_{m,p,q}^{n+\frac{1}{2}}}{\Delta y} \right) \right]}{\left(1 + \frac{\Delta t \sigma}{\varepsilon} \right)} \quad (54)$$

$$H_x \Big|_{m,p,q}^{n+\frac{3}{2}} = H_x \Big|_{m,p,q}^{n+\frac{1}{2}} + \frac{\Delta t}{\mu} \left[\frac{E_y \Big|_{m,p,q+1}^{n+1} - E_y \Big|_{m,p,q}^{n+1}}{\Delta z} \right] - \frac{\Delta t}{\mu} \left[\frac{E_z \Big|_{m,p+1,q}^{n+1} - E_z \Big|_{m,p,q}^{n+1}}{\Delta y} \right] \quad (55)$$

$$H_y \Big|_{m,p,q}^{n+\frac{3}{2}} = H_y \Big|_{m,p,q}^{n+\frac{1}{2}} + \frac{\Delta t}{\mu} \left[\frac{E_z \Big|_{m+1,p,q}^{n+1} - E_z \Big|_{m,p,q}^{n+1}}{\Delta x} \right] - \frac{\Delta t}{\mu} \left[\frac{E_x \Big|_{m,p,q+1}^{n+1} - E_x \Big|_{m,p,q}^{n+1}}{\Delta z} \right] \quad (56)$$

$$H_z \Big|_{m,p,q}^{n+\frac{3}{2}} = H_z \Big|_{m,p,q}^{n+\frac{1}{2}} + \frac{\Delta t}{\mu} \left[\frac{E_x \Big|_{m,p+1,q}^{n+1} - E_x \Big|_{m,p,q}^{n+1}}{\Delta y} \right] - \frac{\Delta t}{\mu} \left[\frac{E_y \Big|_{m+1,p,q}^{n+1} - E_y \Big|_{m,p,q}^{n+1}}{\Delta x} \right] \quad (57)$$

4.3. Boundary Conditions

The FDTD equations (52) to (57) are such that each of the explicit electric/magnetic field equations require values for the magnetic/electric field around (spatially) the point being considered. As such, the arrangement of the Yee cells within the computational grid will result in a ‘missing’ electric/magnetic field at the edge of the computational domain, as demonstrated in Figure 7, representing the $y = 0$ plane: -

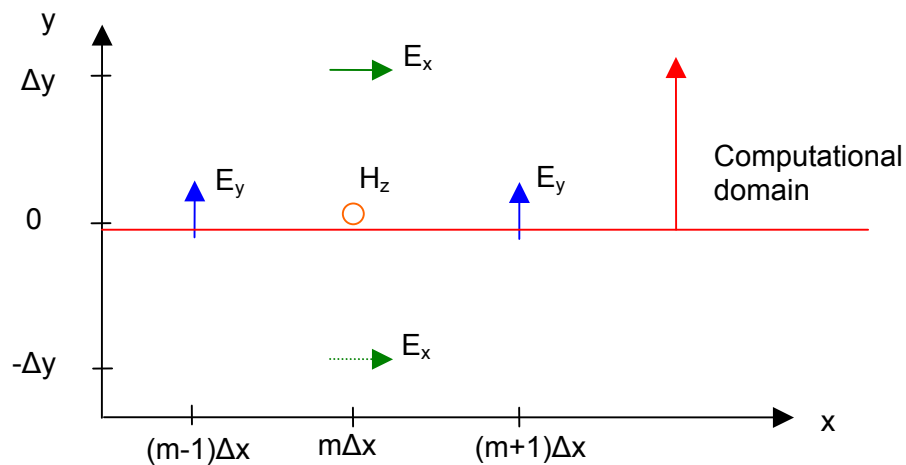


Figure 7: Schematic of edge of computational domain

In this case it can be seen that the $y=-\Delta y$ value is unavailable (i.e. not in the domain and hence not assigned a value) for the FDTD calculation. To negate this effect, we use the Mur boundary condition.

4.3.1. Mur Boundary Conditions

At the edge of the computational grid, the Mur boundary condition [11] uses the previous values on the boundary and interior values of the electric/magnetic fields to determine the grid point values at the boundary. Essentially this uses the assumption that the electromagnetic wave incident on the boundary continues to propagate out of the region at the speed of light, c . Explicitly the first order Mur approximations for the boundaries of the computational domain are given by equations (58) to (69): -

$x=0$

$$H_y|_{0,p,q}^{n+1} = H_y|_{1,p,q}^n + \frac{c\Delta t - \Delta x}{c\Delta t + \Delta x} \left(H_y|_{1,p,q}^{n+1} - H_y|_{0,p,q}^n \right) , \quad (58)$$

$$H_z|_{0,p,q}^{n+1} = H_z|_{1,p,q}^n + \frac{c\Delta t - \Delta x}{c\Delta t + \Delta x} \left(H_z|_{1,p,q}^{n+1} - H_z|_{0,p,q}^n \right) , \quad (59)$$

$y=0$

$$H_x|_{m,0,q}^{n+1} = H_x|_{m,1,q}^n + \frac{c\Delta t - \Delta y}{c\Delta t + \Delta y} \left(H_x|_{m,1,q}^{n+1} - H_x|_{m,0,q}^n \right) , \quad (60)$$

$$H_z|_{m,0,q}^{n+1} = H_z|_{m,1,q}^n + \frac{c\Delta t - \Delta y}{c\Delta t + \Delta y} \left(H_z|_{m,1,q}^{n+1} - H_z|_{m,0,q}^n \right) , \quad (61)$$

$z=0$

$$H_x|_{m,p,0}^{n+1} = H_x|_{m,p,1}^n + \frac{c\Delta t - \Delta z}{c\Delta t + \Delta z} \left(H_x|_{m,p,1}^{n+1} - H_x|_{m,p,0}^n \right) , \quad (62)$$

$$H_y|_{m,p,0}^{n+1} = H_y|_{m,p,1}^n + \frac{c\Delta t - \Delta z}{c\Delta t + \Delta z} \left(H_y|_{m,p,1}^{n+1} - H_y|_{m,p,0}^n \right) , \quad (63)$$

x=MΔx

$$E_y|_{M,p,q}^{n+1} = E_y|_{M-1,p,q}^n + \frac{c\Delta t - \Delta x}{c\Delta t + \Delta x} \left(E_y|_{M-1,p,q}^{n+1} - E_y|_{M,p,q}^n \right) , \quad (64)$$

$$E_z|_{M,p,q}^{n+1} = E_z|_{M-1,p,q}^n + \frac{c\Delta t - \Delta x}{c\Delta t + \Delta x} \left(E_z|_{M-1,p,q}^{n+1} - E_z|_{M,p,q}^n \right) , \quad (65)$$

y=PΔy

$$E_x|_{m,p,q}^{n+1} = E_x|_{m,p-1,q}^n + \frac{c\Delta t - \Delta y}{c\Delta t + \Delta y} \left(E_x|_{m,p-1,q}^{n+1} - E_x|_{m,p,q}^n \right) , \quad (66)$$

$$E_z|_{m,p,q}^{n+1} = E_z|_{m,p-1,q}^n + \frac{c\Delta t - \Delta y}{c\Delta t + \Delta y} \left(E_z|_{m,p-1,q}^{n+1} - E_z|_{m,p,q}^n \right) , \quad (67)$$

z=QΔz

$$E_x|_{m,p,Q}^{n+1} = E_x|_{m,p,Q-1}^n + \frac{c\Delta t - \Delta z}{c\Delta t + \Delta z} \left(E_x|_{m,p,Q-1}^{n+1} - E_x|_{m,p,Q}^n \right) , \quad (68)$$

$$E_y|_{m,p,Q}^{n+1} = E_y|_{m,p,Q-1}^n + \frac{c\Delta t - \Delta z}{c\Delta t + \Delta z} \left(E_y|_{m,p,Q-1}^{n+1} - E_y|_{m,p,Q}^n \right) . \quad (69)$$

4.4. Incident Wave

To determine the backscatter of an incident electromagnetic wave on the object, an incident region of electric and magnetic fields is generated which will travel towards the object to be interrogated through the Yee grid.

Figure 8 shows the arrangement in terms of the incident wave direction: -

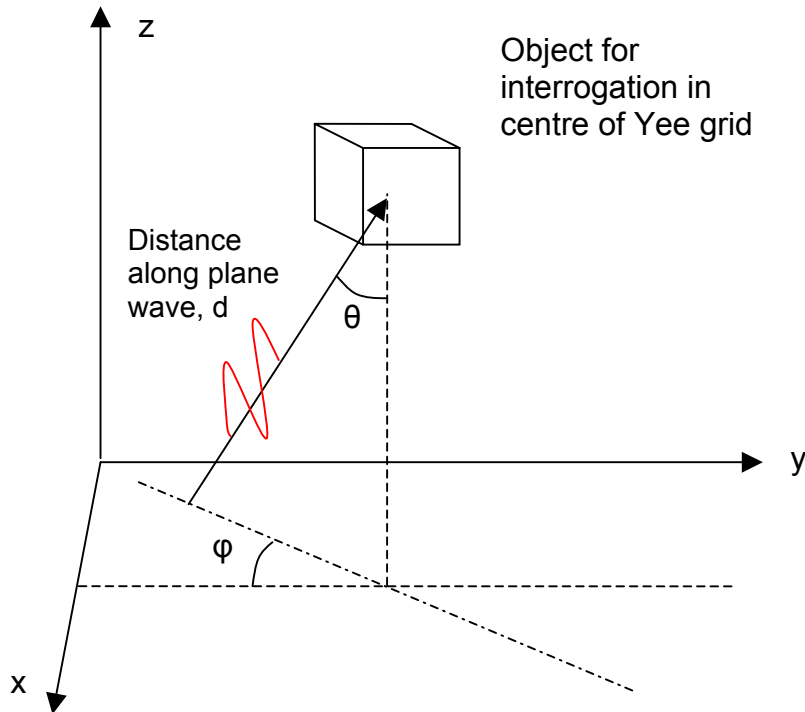


Figure 8: Arrangement of incident wave relative to computational grid

The incident wave will be varied such that it approaches the object from various angles relative to the z-direction in the grid, denoted by θ . This will allow the back-scattered radiation from different aspect angles to be determined, i.e. to give an electric field profile against aspect (viewing) angle. The incident wave will also be rotated about the z-axis, denoted by φ , such that the effect of the Yee grid, i.e. of using a series of cubes to represent a smooth object, can be negated by averaging over these viewing angles. We introduce three Euler angles: -

ψ – a rotation of the incident beam electric and magnetic fields in the x-y plane,

θ – a rotation of the incident beam direction in the y-z plane,

φ – a rotation of the incident beam direction in the x-y plane.

As finite differences are being used in this simulation, discontinuities in electric and/or magnetic fields will tend to produce spurious results and as such a wave that is 'square' (finite in size with zero values on its boundary) will propagate in several directions and be incoherent after a few time steps.

In this problem the incident wave is chosen to be a cylindrical wave, which is Gaussian in a radial direction and spatially along the initial wave. A schematic of this is shown in Figure 9: -

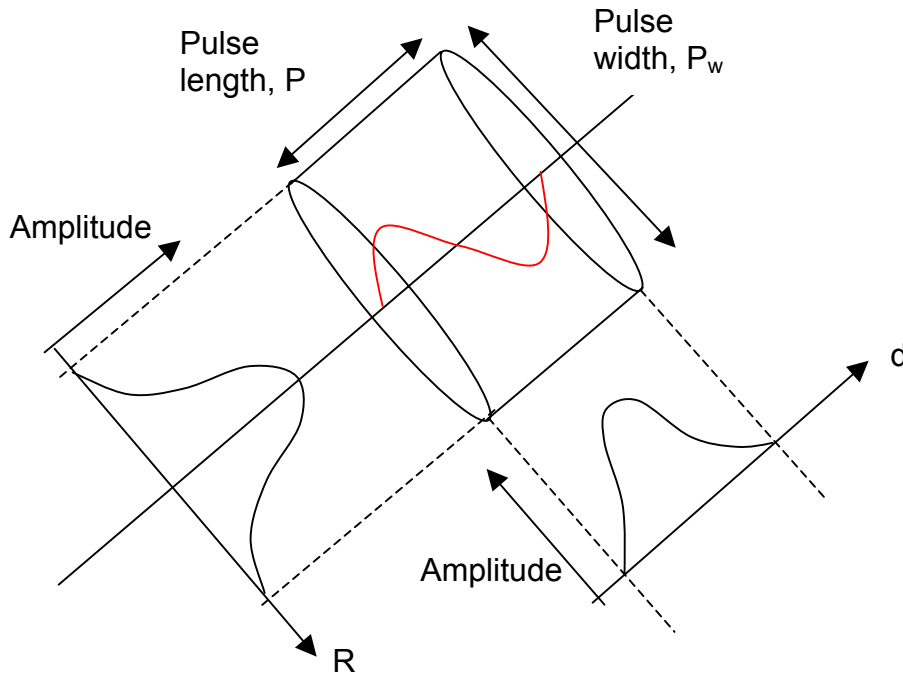


Figure 9: Schematic of incident radar pulse, showing radial and spatial amplitudes

This arrangement for the incident wave is intended to reduce the spurious behaviour at the edge of the wave packet. The amplitude factors, α (along direction of travel) and β (radial from centre of packet) are given by: -

$$\alpha(d) = \exp\left(-\frac{16}{P^2}\left(d - \frac{P}{2}\right)^2\right) \quad (70)$$

$$\beta(r) = \exp\left(-\frac{16}{P_w^2}R^2\right) \quad (71)$$

The factor of 16 gives a value of 1.1×10^{-7} at the edge of the pulse, which is believed to be sufficient to truncate the pulse region.

The parameters R and d are determined by considering a unit vector, \underline{u} , which describes the Poynting vector (see section 2.1.) and specifies the desired direction of propagation of the incident wave, given in spherical coordinates by: -

$$u_x = -\sin \varphi \sin \theta \quad , \quad (72)$$

$$u_y = -\cos \varphi \sin \theta \quad , \quad (73)$$

$$u_z = -\cos \theta \quad , \quad (74)$$

where φ and θ are the angles shown in Figure 8. For any point in the Yee grid, \underline{r} , the dot product with this unit vector allows us to determine the distance of the point in terms of a parallel and normal component to the \underline{u} vector. This then allows the radial and spatial amplitude factors to be determined and applied to the peak amplitudes.

The incident wave will be polarised (in electric field) at an angle, ψ , relative to the z-axis. We arbitrarily take the incident electric field to be defined by the peak amplitude in the y electric field component, given by E_0 . To produce expressions for the incident wave at any direction relative to the grid, we use a rotation matrix to denote the three transformations from this initial electric field: -

$$\begin{bmatrix} E_x \\ E_y \\ E_z \end{bmatrix} = \begin{bmatrix} \cos \varphi & \sin \varphi & 0 \\ -\sin \varphi & \cos \varphi & 0 \\ 0 & 0 & 1 \end{bmatrix} \begin{bmatrix} 1 & 0 & 0 \\ 0 & \cos \theta & \sin \theta \\ 0 & -\sin \theta & \cos \theta \end{bmatrix} \begin{bmatrix} \cos \psi & \sin \psi & 0 \\ -\sin \psi & \cos \psi & 0 \\ 0 & 0 & 1 \end{bmatrix} \begin{bmatrix} 0 \\ E_0 \\ 0 \end{bmatrix} . \quad (75)$$

As the subsequent numerical analysis will be based on the amplitude of the electric field back-scattered compared to the incident electric field amplitude, we defined the initial electric field amplitude, E_0 , and determine the initial magnitude of the magnetic field, H_0 , by equation (76) [3]: -

$$H_0 = \frac{E_0}{\nu} , \quad (76)$$

$$\text{where, } \nu = \sqrt{\frac{\mu_0}{\varepsilon_0}}, \quad (77)$$

gives the free space impedance. Combining this information with the transformation defined in (75) we can derive the six initial wave amplitudes in the x, y and z component directions: -

$$\begin{aligned} E_x &= E_0 (\sin \psi \cos \varphi + \cos \psi \cos \theta \sin \varphi) & H_x &= -\frac{E_0}{\nu} (\cos \psi \cos \varphi - \sin \psi \cos \theta \sin \varphi) \\ E_y &= E_0 (-\sin \psi \sin \varphi + \cos \psi \cos \theta \cos \varphi) & H_y &= -\frac{E_0}{\nu} (-\cos \psi \sin \varphi - \sin \psi \cos \theta \cos \varphi) \\ E_z &= E_0 (-\cos \psi \sin \theta) & H_z &= -\frac{E_0}{\nu} (\sin \psi \sin \theta) \end{aligned} \quad . (78)$$

The approximation we will use in the formulation of the incident electric field wave can be explicitly described as: -

$$E_x|_{m,p,q}^0 \approx E_x(\underline{r}), \quad (79)$$

$$\text{where } \underline{r} = \underline{i}(m\Delta x) + \underline{j}(p\Delta y) + \underline{k}(q\Delta z). \quad (80)$$

The spatial components of the wave in the initial conditions of the problem are given by (81) and (82), and are derived from the analytical solution of a plane wave travelling in free space (see section 3.1.): -

$$E_y|_{m,p,q}^{n=0} = E_0 \cos\left(\frac{2\pi}{\lambda} |\underline{r}|\right), \quad (81)$$

$$H_x|_{m,p,q}^{n=\frac{1}{2}} = -\frac{E_0}{\nu} \cos\left(\frac{2\pi}{\lambda} |\underline{r}| + \frac{c\Delta t}{2}\right), \quad (82)$$

$$\text{where } |\underline{r}| = \left((m\Delta x)^2 + (p\Delta y)^2 + (q\Delta z)^2\right)^{\frac{1}{2}}. \quad (83)$$

As the FDTD is a leapfrog approach, consideration must be given to the initial conditions to represent this process, in this case we require the initial incident wave to represent the analytical plane wave solution for the electric field at time n=0, and the magnetic field at time n=1/2. Here, the magnetic field is negative so

that the correct Poynting vector is obtained such that the initial wave propagates from the outside of the Yee grid towards the object.

When expressions (75), (81) and (82) are combined, the initial electric and magnetic fields are specified by: -

$$E_x|_{\underline{r}}^{n=0} = E_0 \alpha(d(\underline{r})) \beta(\underline{r}) (\sin \psi \cos \varphi + \cos \psi \cos \theta \sin \varphi) \cos\left(\frac{2\pi d(\underline{r})}{\lambda}\right) \quad (84)$$

$$E_y|_{\underline{r}}^{n=0} = E_0 \alpha(d(\underline{r})) \beta(\underline{r}) (-\sin \psi \sin \varphi + \cos \psi \cos \theta \cos \varphi) \cos\left(\frac{2\pi d(\underline{r})}{\lambda}\right) \quad (85)$$

$$E_z|_{\underline{r}}^{n=0} = E_0 \alpha(d(\underline{r})) \beta(\underline{r}) (-\cos \psi \sin \theta) \cos\left(\frac{2\pi d(\underline{r})}{\lambda}\right) \quad (86)$$

$$H_x|_{\underline{r}}^{n=\frac{1}{2}} = -\frac{E_0}{\nu} \alpha\left(d(\underline{r}) + \frac{c\Delta t}{2}\right) \beta(\underline{r}) (\cos \psi \cos \varphi - \sin \psi \cos \theta \sin \varphi) \cos\left(\frac{2\pi d(\underline{r})}{\lambda} + \frac{c\Delta t}{2}\right) \quad (87)$$

$$H_y|_{\underline{r}}^{n=\frac{1}{2}} = -\frac{E_0}{\nu} \alpha\left(d(\underline{r}) + \frac{c\Delta t}{2}\right) \beta(\underline{r}) (-\cos \psi \sin \varphi - \sin \psi \cos \theta \cos \varphi) \cos\left(\frac{2\pi d(\underline{r})}{\lambda} + \frac{c\Delta t}{2}\right) \quad (88)$$

$$H_z|_{\underline{r}}^{n=\frac{1}{2}} = -\frac{E_0}{\nu} \alpha\left(d(\underline{r}) + \frac{c\Delta t}{2}\right) \beta(\underline{r}) (\sin \psi \sin \theta) \cos\left(\frac{2\pi d(\underline{r})}{\lambda} + \frac{c\Delta t}{2}\right) \quad (89)$$

Here, $d(\underline{r})$ denotes the distance of the point \underline{r} along the direction of travel from the origin of the wave, $\alpha(d(\underline{r}))$ and $\beta(\underline{r})$ represent the parallel and orthogonal amplitude factors respectively at the point \underline{r} .

4.5. Non-time Harmonic Electromagnetic Wave

A radar system may vary the rate of change of electric field generation from its radiating elements as it emits radiation. Consequently this varies the wavelength of the radio waves emitted from the radar, and as such a single pulse may have numerous sections of non equal wavelengths throughout its pulse. In particular, a typical radar technique known as ‘chirping’ (see [5] for details) increases or decreases the wavelength of the generated radio waves linearly with time. A description of the radar processing of a received chirped pulse is available in

[14]. This is known as up chirping (decreasing λ with time) and down chirping (increasing λ with time). A schematic of these processes is shown in Figure 10: -

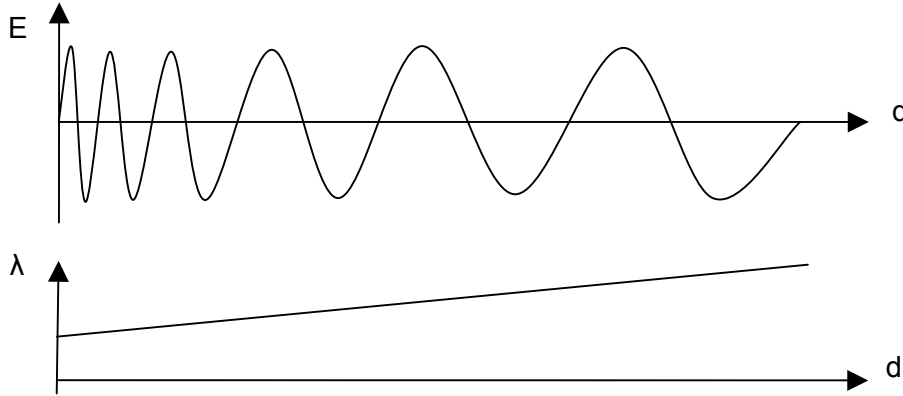


Figure 10: Schematic of a down chirp radio wave

Given that the wavelength of the radio wave through the pulse can be expressed as: -

$$\lambda(d) = \lambda_0 + \lambda'd, \quad (90)$$

where: -

$\lambda(d)$ = Wavelength at distance d along pulse,

λ_0 = Wavelength at front of pulse (d=0),

λ' = Rate of change of wavelength with distance (positive or negative).

We can therefore modify equation (84) to include a chirp: -

$$E_x|_r^{n=0} = E_0 \alpha(\underline{r}) \beta(\underline{r}) (\sin \psi \cos \varphi + \cos \psi \cos \theta \sin \varphi) \cos \left(\frac{2\pi d(\underline{r})}{\lambda_0 + \lambda' d(\underline{r})} \right), \quad (91)$$

and similarly equations (84) to (89) can be modified to include the chirp term.

This formulation for the initial electric and magnetic fields will be used for the analysis in section 7.

4.6. Truncation Error

Truncation error is the error introduced into the numerical solution caused by the approximation of using the scheme (in this case the FDTD method) instead of the analytical formula. In this case the truncation error, $\tau_{m,p,q}^n$, is expressed mathematically by: -

$$L(H_x) = \mu \frac{\partial H_x|_{x,y,z}^t}{\partial t} - \frac{\partial E_y|_{x,y,z}^t}{\partial z} + \frac{\partial E_z|_{x,y,z}^t}{\partial y}, \quad (92)$$

$$L_h(H_x|_{m,p,q}^n) = \mu \frac{H_x|_{m,p,q}^{n+1} - H_x|_{m,p,q}^n}{\Delta t} - \frac{E_y|_{m,p,q+\frac{1}{2}}^{n+\frac{1}{2}} - E_y|_{m,p,q-\frac{1}{2}}^{n+\frac{1}{2}}}{\Delta z} + \frac{E_z|_{m,p+\frac{1}{2},q}^{n+\frac{1}{2}} - E_z|_{m,p-\frac{1}{2},q}^{n+\frac{1}{2}}}{\Delta y}, \quad (93)$$

$$\tau_{m,p,q}^n \equiv L_h(H_x) - L_h(H_x|_{m,p,q}^n), \quad (94)$$

$$\tau_{m,p,q}^n = L_h(H_x) - 0. \quad (95)$$

Theorem

The leading term of the truncation error is given by: -

$$\tau_{m,p,q}^{n+\frac{1}{2}} = \frac{\mu \Delta t^2}{24} \frac{\partial^3}{\partial t^3} \left(H_x|_{m,p,q}^{n+\frac{1}{2}} \right) - \frac{\Delta z^2}{24} \frac{\partial^3}{\partial z^3} \left(E_y|_{m,p,q}^{n+\frac{1}{2}} \right) + \frac{\Delta y^2}{24} \frac{\partial^3}{\partial y^3} \left(E_z|_{m,p,q}^{n+\frac{1}{2}} \right) + \dots \quad (96)$$

The truncation error is second order in both space and time and hence the scheme is consistent, i.e. the numerical solution will tend to the exact (analytical) solution as the temporal timesteps and spatial grid spacing tend to zero.

Proof

We expand H_x , E_y and E_z from equation (93) about the point $((n+1/2)\Delta t, m\Delta x, p\Delta y, q\Delta z)$: -

$$\tau_{m,p,q}^{n+\frac{1}{2}} = \frac{\mu}{\Delta t} \left[H_x|_{m,p,q}^{n+1} - H_x|_{m,p,q}^n \right] - \frac{1}{\Delta z} \left[E_y|_{m,p,q+\frac{1}{2}}^{n+\frac{1}{2}} - E_y|_{m,p,q-\frac{1}{2}}^{n+\frac{1}{2}} \right] + \frac{1}{\Delta y} \left[E_z|_{m,p+\frac{1}{2},q}^{n+\frac{1}{2}} - E_z|_{m,p-\frac{1}{2},q}^{n+\frac{1}{2}} \right], \quad (97)$$

$$\begin{aligned} \tau_{m,p,q}^{n+\frac{1}{2}} &= \frac{\mu}{\Delta t} \left[H_x|_{m,p,q}^{n+\frac{1}{2}} + \frac{\Delta t}{2} \frac{\partial}{\partial t} \left(H_x|_{m,p,q}^{n+\frac{1}{2}} \right) + \frac{\Delta t^2}{8} \frac{\partial^2}{\partial t^2} \left(H_x|_{m,p,q}^{n+\frac{1}{2}} \right) + \frac{\Delta t^3}{48} \frac{\partial^3}{\partial t^3} \left(H_x|_{m,p,q}^{n+\frac{1}{2}} \right) + \dots \right] \\ &- \frac{\mu}{\Delta t} \left[H_x|_{m,p,q}^{n+\frac{1}{2}} - \frac{\Delta t}{2} \frac{\partial}{\partial t} \left(H_x|_{m,p,q}^{n+\frac{1}{2}} \right) + \frac{\Delta t^2}{8} \frac{\partial^2}{\partial t^2} \left(H_x|_{m,p,q}^{n+\frac{1}{2}} \right) - \frac{\Delta t^3}{48} \frac{\partial^3}{\partial t^3} \left(H_x|_{m,p,q}^{n+\frac{1}{2}} \right) + \dots \right] \\ &- \frac{1}{\Delta z} \left[E_y|_{m,p,q}^{n+\frac{1}{2}} + \frac{\Delta z}{2} \frac{\partial}{\partial z} \left(E_y|_{m,p,q}^{n+\frac{1}{2}} \right) + \frac{\Delta z^2}{8} \frac{\partial^2}{\partial z^2} \left(E_y|_{m,p,q}^{n+\frac{1}{2}} \right) + \frac{\Delta z^3}{48} \frac{\partial^3}{\partial z^3} \left(E_y|_{m,p,q}^{n+\frac{1}{2}} \right) + \dots \right] \\ &+ \frac{1}{\Delta z} \left[E_y|_{m,p,q}^{n+\frac{1}{2}} - \frac{\Delta z}{2} \frac{\partial}{\partial z} \left(E_y|_{m,p,q}^{n+\frac{1}{2}} \right) + \frac{\Delta z^2}{8} \frac{\partial^2}{\partial z^2} \left(E_y|_{m,p,q}^{n+\frac{1}{2}} \right) - \frac{\Delta z^3}{48} \frac{\partial^3}{\partial z^3} \left(E_y|_{m,p,q}^{n+\frac{1}{2}} \right) + \dots \right] \\ &+ \frac{1}{\Delta y} \left[E_z|_{m,p,q}^{n+\frac{1}{2}} + \frac{\Delta y}{2} \frac{\partial}{\partial y} \left(E_z|_{m,p,q}^{n+\frac{1}{2}} \right) + \frac{\Delta y^2}{8} \frac{\partial^2}{\partial y^2} \left(E_z|_{m,p,q}^{n+\frac{1}{2}} \right) + \frac{\Delta y^3}{48} \frac{\partial^3}{\partial y^3} \left(E_z|_{m,p,q}^{n+\frac{1}{2}} \right) + \dots \right] \\ &- \frac{1}{\Delta y} \left[E_z|_{m,p,q}^{n+\frac{1}{2}} - \frac{\Delta y}{2} \frac{\partial}{\partial y} \left(E_z|_{m,p,q}^{n+\frac{1}{2}} \right) + \frac{\Delta y^2}{8} \frac{\partial^2}{\partial y^2} \left(E_z|_{m,p,q}^{n+\frac{1}{2}} \right) - \frac{\Delta y^3}{48} \frac{\partial^3}{\partial y^3} \left(E_z|_{m,p,q}^{n+\frac{1}{2}} \right) + \dots \right] \end{aligned} \quad (98)$$

$$\begin{aligned} &= \frac{\mu}{\Delta t} \left[\Delta t \frac{\partial}{\partial t} \left(H_x|_{m,p,q}^{n+\frac{1}{2}} \right) + \frac{\Delta t^3}{24} \frac{\partial^3}{\partial t^3} \left(H_x|_{m,p,q}^{n+\frac{1}{2}} \right) + \dots \right] \\ &- \frac{1}{\Delta z} \left[\Delta z \frac{\partial}{\partial z} \left(E_y|_{m,p,q}^{n+\frac{1}{2}} \right) + \frac{\Delta z^3}{24} \frac{\partial^3}{\partial z^3} \left(E_y|_{m,p,q}^{n+\frac{1}{2}} \right) + \dots \right] \\ &+ \frac{1}{\Delta y} \left[\Delta y \frac{\partial}{\partial y} \left(E_z|_{m,p,q}^{n+\frac{1}{2}} \right) + \frac{\Delta y^3}{24} \frac{\partial^3}{\partial y^3} \left(E_z|_{m,p,q}^{n+\frac{1}{2}} \right) + \dots \right] \end{aligned} \quad (99)$$

$$\begin{aligned} &= \mu \frac{\partial}{\partial t} \left(H_x|_{m,p,q}^{n+\frac{1}{2}} \right) - \frac{\partial}{\partial z} \left(E_y|_{m,p,q}^{n+\frac{1}{2}} \right) + \frac{\partial}{\partial y} \left(E_z|_{m,p,q}^{n+\frac{1}{2}} \right) + \frac{\mu \Delta t^2}{24} \frac{\partial^3}{\partial t^3} \left(H_x|_{m,p,q}^{n+\frac{1}{2}} \right) \\ &- \frac{\Delta z^2}{24} \frac{\partial^3}{\partial z^3} \left(E_y|_{m,p,q}^{n+\frac{1}{2}} \right) + \frac{\Delta y^2}{24} \frac{\partial^3}{\partial y^3} \left(E_z|_{m,p,q}^{n+\frac{1}{2}} \right) + \dots \end{aligned} \quad (100)$$

With the original PDE we can remove the first three zeroth order terms, and the result follows. ■

A similar analysis to this can be performed on all six FDTD equations used in the scheme, and by inspection we can see that we will obtain the same conclusion, i.e. second order in space and time, from each expression (46) – (51).

4.7. Stability

The stability condition of the FDTD is given by the Courant condition, which determines the maximum time step to be used given a known grid spacing [1]: -

$$\Delta t \leq c^{-1} \left(\frac{1}{\Delta x^2} + \frac{1}{\Delta y^2} + \frac{1}{\Delta z^2} \right)^{-1/2}. \quad (101)$$

In the subsequent analysis, we use the expression below for the time step: -

$$\Delta t = 0.9c^{-1} \left(\frac{1}{\Delta x^2} + \frac{1}{\Delta y^2} + \frac{1}{\Delta z^2} \right)^{-1/2}, \quad (102)$$

and as we will be using the same grid spacing in each axis ($\Delta x = \Delta y = \Delta z$), this reduces down to: -

$$\Delta t = 0.9c^{-1} \frac{\Delta y}{\sqrt{3}}, \quad (103)$$

where we have chosen to define the three grid spacings in terms of the grid spacing along the y-axis.

4.8. Choice of Grid Spacing

When modelling a wave in a finite difference code, it is often suggested that a suitable approximation to a sine wave consists of at least 10 numerical points along a full wavelength [1], as shown in Figure 11: -

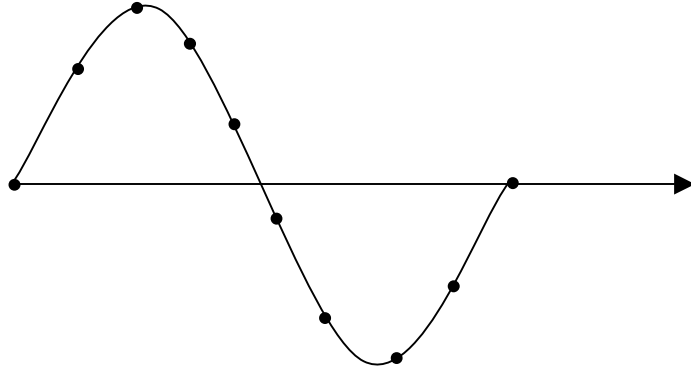


Figure 11: Suggested numerical sampling of incident wave

So to model a plane wave (wavelength λ) travelling in the y direction in free space through the domain modelled, we could choose Δy to be equal to $\lambda/10$. However, as well as travelling through free space we also want to consider the propagation and associated backscatter from dielectric lossy materials, which have a relative permittivity which will produce a change in the wavelength of the electromagnetic wave. The change in wavelength is given by equation (33). Therefore we assign the grid spacing based on the permittivities found within our computational domain, D: -

$$\Delta x = \Delta y = \Delta z = \min_{r \in D} \left\{ \frac{\lambda_i}{10\sqrt{\epsilon_r(r)}} \right\}. \quad (104)$$

This condition is used to determine the minimum grid spacing when modelling harmonic waves within the FDTD code. An investigation into the use of this condition for non-time harmonic waves is presented in section 7.

When considering radar, we often describe the frequency of the radio wave from the radar in terms of its 'band', which cover a range of frequencies. In this project we will be considering VHF to X-band, which covers the frequency range 200 MHz to 3 GHz. So the grid spacing used will be in the order of centimetres (10^{-2} m) and hence the time steps will be of the order of tens of picoseconds (10^{-12} s).

5. Plasma Theory

The term plasma refers to a gas which has been excited by some method such that there is a dissociation of electrons from atoms and/or molecules such that charged (positive and negative) and neutral ions exist. The distinguishing feature between plasma and an ordinary ionised gas is that plasma experiences collective behaviour, explicitly this is due to the alternating electric fields generated in the plasma which affect the particles in the plasma locally but also affect charged particles at a distance [2].

Plasmas may be generated naturally by objects passing rapidly through the Earth's atmosphere (meteorites, de-orbiting satellites) and by incident solar radiation acting upon the ionosphere. Plasmas may be generated artificially by the use of an electron gun.

There are several categories of plasma that have different characteristics. Collisions of charge carriers in plasma are associated with the conductivity of the plasma. Cold plasmas denote those plasmas where the number of collisions (parameterised by the collision frequency, ν_c , given in collisions per second (Hz)) between ions is low. Hot plasmas have a large value for ν_c , and therefore have an appreciable current density, such that it is significant compared to the induced current when an electromagnetic wave is incident on the plasma.

Considering the situation where a layer of positive and negative ions have dissociated within plasma as shown in Figure 12: -

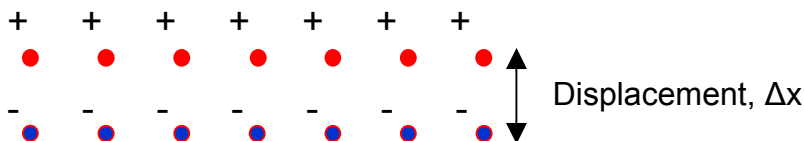


Figure 12: Arrangement of dissociated ionized plasma

Given a displacement, Δx , between the positive and negative 'slabs' a potential difference will exist between these two regions, resulting in an electric field acting on both layers. The equation of motion is of the form

$$F = m \frac{\partial^2 x}{\partial t^2} = Ax, \quad (105)$$

where A incorporates the electric permittivity of the region between the electric charges involved. Clearly this equation is that of an oscillatory system, and as such a parameter known as the plasma frequency, ω_f , is introduced to describe this motion. When considering the formation and motion of plasma, it is often considered that the positive/neutral ions within the plasma are stationary, and the electrons are the only particles which exhibit the oscillatory behaviour as described by (105). This is a good approximation as the mass of the electron is 1/1836 that of a hydrogen atom (the lightest constituent of the Earth's atmospheric gases), so that the electrons oscillate rapidly with respect to the other constituents of the plasma.

Plasma is characterised by its Total Electron Content (TEC), which describes the number of free electrons within a given volume, and the collision frequency between ions. The TEC can be used to estimate plasma frequency, using the expression [2]: -

$$\omega_f = \sqrt{\frac{e^2 N_e}{m_e \epsilon_0}}, \quad (106)$$

where ω_f has the units of radians per second, N_e is TEC, m_e is the mass of an electron, e and ϵ_0 are fundamental constants (electron charge and permittivity of free space respectively).

To determine the effect of an electromagnetic wave incident on a plasma, we must quantify the plasma using the complex permittivity [3], ϵ_c , which can vary so that we get a distribution for the complex permittivity relative to position within the plasma, \underline{r} , i.e. that: -

$$\epsilon_c = \epsilon_c(\underline{r}) = \epsilon'(\underline{r}) - i\epsilon''(\underline{r}), \quad (107)$$

where $i = \sqrt{-1}$.

The real part of the complex permittivity, $\epsilon'(\underline{r})$, gives the effect of the plasma on the polarisation of the propagating electromagnetic wave, i.e. it gives the relative permittivity of the medium, ϵ_r . The imaginary part, $\epsilon''(\underline{r})$, describes how the amplitude of an incident electromagnetic wave varies as it propagates through the medium, and is related to the conductivity, σ , by: -

$$\epsilon''(\underline{r}) = \frac{\sigma(\underline{r})}{\omega}, \quad (108)$$

where ω is the frequency of the wave incident on the plasma, expressed in radians per second.

A generic expression for the complex permittivity of plasma in terms of the plasma frequency and collision frequency (ν_c) is given by [3]: -

$$\epsilon' = 1 - \frac{\omega_f^2}{\omega^2 + \nu_c^2}, \quad (109)$$

$$\epsilon'' = \frac{\nu_c}{\omega} \frac{\omega_f^2}{\omega^2 + \nu_c^2}. \quad (110)$$

5.1. Cold plasma

In the case of cold plasmas where the collision frequency is low, the electric current density tends to zero, and the conductivity of the plasma can be neglected. An example of cold plasma is the Earth's ionosphere [12]. The plasma frequencies for principle constituents of the ionosphere are of the order 10^5 to 10^7 Hz [12]. Considering VHF radio waves of frequency 100 MHz incident on the ionosphere, the electric permittivity of the ionosphere is of the order: -

$$\max(\varepsilon_r) = \varepsilon' \approx 1 - \left(\frac{10^5}{10^8}\right)^2$$

$$\therefore \max(\varepsilon_r) \approx 0.999999$$

$$\min(\varepsilon_r) = \varepsilon' \approx 1 - \left(\frac{10^7}{10^8}\right)^2$$

$$\therefore \min(\varepsilon_r) \approx 0.99$$

and as discussed above only the real part of the complex permittivity is considered.

5.2. Group and Phase Velocity in Plasma

A characteristic, and somewhat surprising, feature of electromagnetic waves propagating through plasma is that the phase velocity of the wave may exceed the value of c , i.e. the peaks in amplitude of the wave propagate faster than the speed of light in a vacuum. This would appear to violate relativistic theory which limits the speed of propagation of electromagnetic waves in a medium to the value of c . The definition of the phase velocity, v_p , is the rate of change of distance with time of a point of constant phase on a wave, explicitly: -

$$\frac{dx}{dt} = \frac{\omega}{k} = v_p \quad (111)$$

The reasoning behind why this does not violate the theory of relativity is that an infinitely long wave train of constant amplitude cannot carry information [2]. For instance the radar wave considered in this project only carries information when a modulation is applied to it. This modulation travels at a velocity less than c , and is quantified by the group velocity, v_g , [2]: -

$$\frac{d\omega}{dk} = \frac{c^2}{v_p} = v_g \quad (112)$$

As the wave propagates in the plasma its wavelength increases as given by the dispersion relation. For an electromagnetic wave propagating in plasma which is

not subject to any external magnetic fields, the dispersion relation for the wave is given by [2]: -

$$\omega^2 = \omega_f^2 + c^2 k^2. \quad (113)$$

This equation says that for an electromagnetic wave of a known frequency, ω , incident on plasma, the wave number, k , will reduce as the plasma frequency, ω_f , increases. Ultimately, as the plasma frequency increases and surpasses the frequency of the incident wave, the plasma no longer allows the wave to propagate (k becomes 0 at $\omega_f = \omega$, then imaginary as ω_f increases further). Therefore plasma whose plasma frequency is greater than that of the incident wave appears opaque to the incident wave.

In section 7 we shall examine the variation of the wavelength of a radar pulse in plasma, so for ease of use we rearrange (113) to give the wavelength, λ_p , in the plasma in terms of the plasma frequency: -

$$\lambda_p = \frac{2\pi c}{(\omega^2 - \omega_f^2)^{1/2}}. \quad (114)$$

6. Numerical Results from Time Harmonic Problem

6.1. Plane Wave in Free Space

Firstly, we examine the case of an electromagnetic wave propagating through free space and analyse the numerical solution for the evolution of our radar pulse within the computational grid, with the permittivity being equal to ϵ_0 ($\epsilon_r = 1$) everywhere in the domain. We examine this case as the analytical solution is known for the whole domain; explicitly that the amplitude, wavelength and spatial extent of the wave will remain constant as it propagates forward.

We take the grid spacing $\Delta x = \Delta y = \Delta z = 0.2$ m, the wavelength $\lambda = 3$ m (100MHz) along with a pulse width, P_w , of 10 m and pulse length, P , of 6 m. Examining the amplitude of the numerical solution for the electric field as time progresses: -

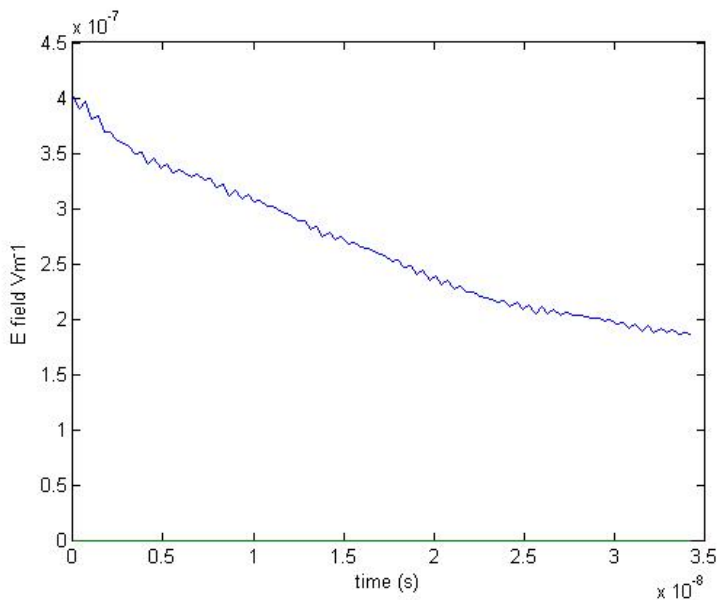


Figure 13: Amplitude of numerical approximation of the electric field of a wave in free space as time progresses

The numerical amplitude reduces with time, and has a rate of change of the order $-6.23 \times 10^{-5} \text{ Vm}^{-1}\text{ps}^{-1}$. This would imply that the initial wave would tend to zero amplitude after 64 ns, i.e. after approximately 190 time steps. Increasing the pulse width of the initial radar pulse region to 15 m: -

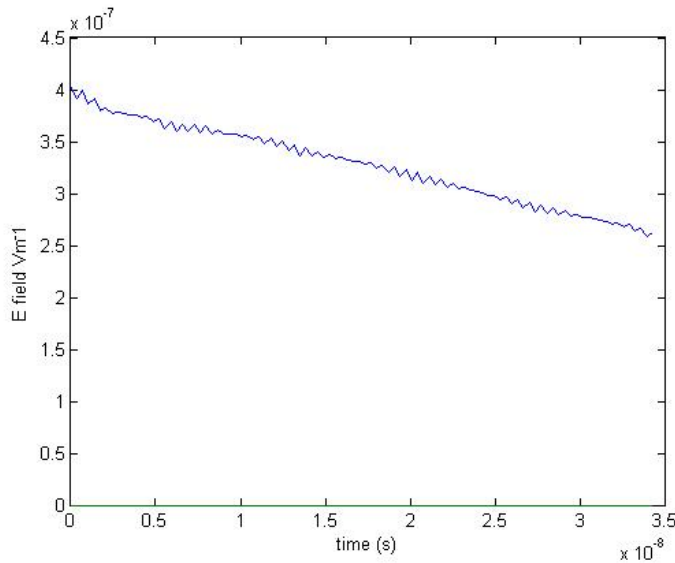


Figure 14: Variation of amplitude with time of the numerical solution for electric field in free space, pulse width = 15 m

The rate of change of electric field amplitude with time in this instance is the order of $-4.08 \times 10^{-5} \text{ Vm}^{-1}\text{ps}^{-1}$. This suggests that a broader beam produces less (artificial) attenuation of the signal at the beam centre.

Part of the reason why attenuation of the electric field is observed in the centre of the beam comes from the use of a Gaussian function in the radial direction to factor the initial electric and magnetic fields within the radar pulse (see section 4.4). From inspection of the Gaussian function (plotted in Figure 15) we can see that as the gradient of the function is non-zero, adjacent electric/magnetic fields along the radius will not be equal, for example considering the H_x field for a wave travelling perpendicular to the z-axis: -

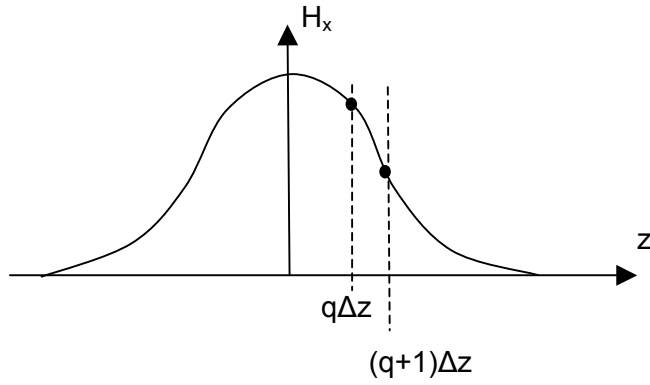


Figure 15: Gaussian distribution schematic

The difference in the H_x field can be expressed as (using equation (87)): -

$$H_x|_{m,p,q}^{n+\frac{1}{2}} - H_x|_{m,p,q+1}^{n+\frac{1}{2}} = \frac{E_0}{\nu} \cos\left(\frac{2\pi d(\underline{r})}{\lambda}\right) \{\beta(\underline{r} + \Delta z) - \beta(\underline{r})\}, \quad (115)$$

$$H_x|_{m,p,q}^{n+\frac{1}{2}} - H_x|_{m,p,q+1}^{n+\frac{1}{2}} = \frac{E_0}{\nu} \cos\left(\frac{2\pi d(\underline{r})}{\lambda}\right) \left\{ \exp\left(\frac{-16}{P_w^2}(r + \Delta r)^2\right) - \exp\left(\frac{-16}{P_w^2}r^2\right) \right\}. \quad (116)$$

Consequently this radial gradient in the initial conditions of H_x causes an effect on the calculation of E_y at the $n = 1$ time step (as described by equation (53)). A normalized plot of the gradient of the Gaussian function is shown in Figure 16: -

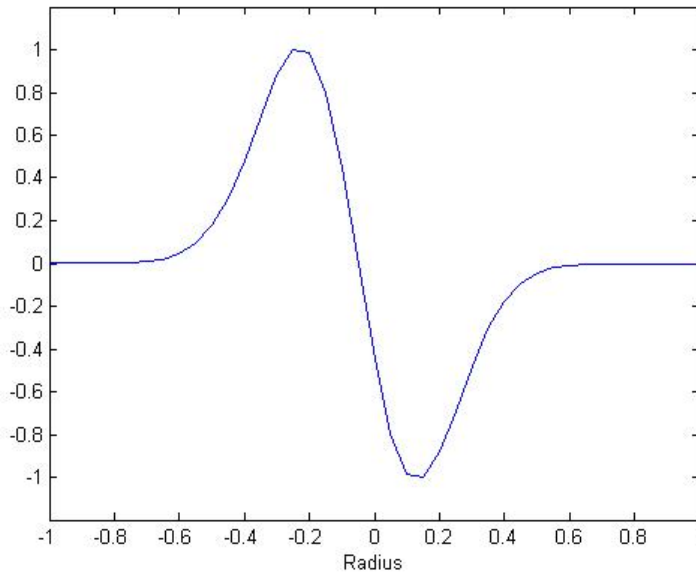


Figure 16: Plot of gradient introduced by radial Gaussian function

In effect this causes the wave to travel not only in the intended direction (in this case perpendicular to the z-direction) but also to disperse in both the positive and negative z directions as time progresses.

6.2. Plane Wave Incident on a Dielectric Medium

The second case considered is when a radar pulse described by a plane wave is incident on an 'infinite' (extending throughout the whole computational domain in the x-z plane) dielectric medium, described by a constant electric permittivity ϵ_r . We consider ϵ_r to take a value of 2, which by using the Snell's laws and Fresnel equations ((28) to (31)) allows a comparison between the analytic to numerical results. The reflected wave when the incident wave is normal to the plane ($\zeta_i = \zeta_t = 0$) will have peak amplitude: -

$$\frac{|E_x^r|}{|E_x^i|} = \frac{(\sqrt{2} \cos 0)^{-1} - (\cos 0)^{-1}}{(\sqrt{2} \cos 0)^{-1} + (\cos 0)^{-1}}$$

$$\frac{|E_x^r|}{|E_x^i|} = \frac{2^{-1/2} - 1}{2^{-1/2} + 1} = -0.1716 \quad . \quad (117)$$

So in this situation the backscatter from the dielectric will experience a change in phase of π radians (due to the minus sign), with peak electric field amplitude 17.16% of the incident field. From the analytical solution we would expect this amplitude to remain constant as it propagates away from the dielectric. We will compare incident fields at 0 and 45 degrees to the normal of the plane of the dielectric region.

6.2.1. Incidence Angle = 0 Degrees

The analytical solution for this situation is derived by considering the centre of the incident wave (i.e. where the electric field is a maximum). The incident electric / magnetic fields are shown in Figure 17: -

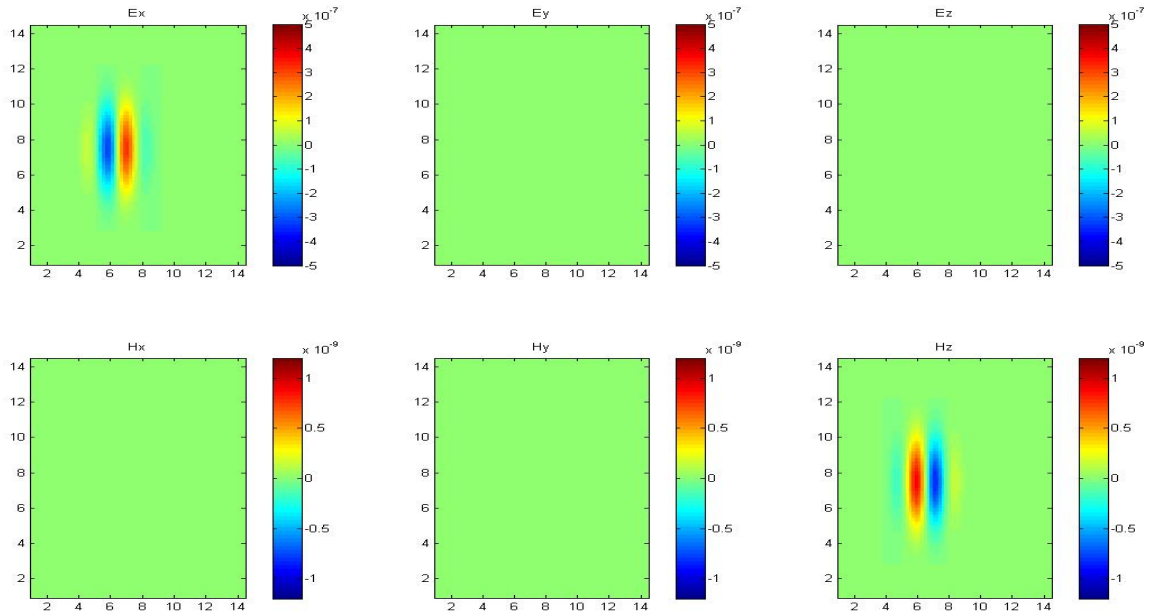


Figure 17: Incident electromagnetic wave in the y-z plane. Electric field is in Vm^{-1} , magnetic field is in Am^{-1} and distances (y, z axes) are in meters.

The electric field is recorded along the line normal to the material. Considering a point at a distance 6.0 m away from the dielectric, the electric field evolution is shown in Figure 18. The analytical solution is also shown (in blue): -

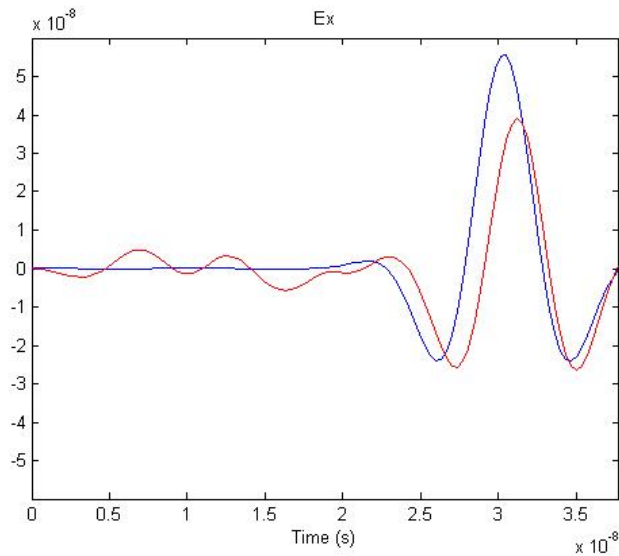


Figure 18: Analytical solution (blue) compared to numerical solution (red) of reflected electric field normally incident on a dielectric ($\epsilon_r = 2$) material.

From the figure it can be seen that although there is some agreement between the shape of the electric field for the numerical and analytic solutions, it appears that there has been some reduction in the wavelength and amplitude of the reflected wave. The change in wavelength that has occurred in the numerical solution was assessed to be $\lambda=2.8\text{m}$ (c.f. 3.0 m wavelength incident), this is shown in Figure 19: -

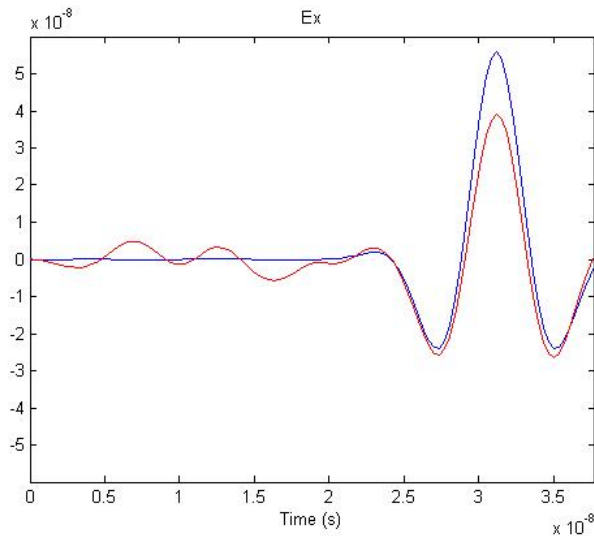


Figure 19: Analytical solution (blue) with $\lambda = 2.8\text{m}$ compared to numerical solution (red) of reflected electric field normally incident on a dielectric ($\epsilon_r = 2$) material.

From this we conclude that the wavelength of the reflected wave off a dielectric is not modelled correctly in the numerical solution. This may be due to the use of the Gaussian function to truncate the radar pulse and is discussed further in 6.3.

The absolute error between the numerical and analytic solution is quantified in Figure 20: -

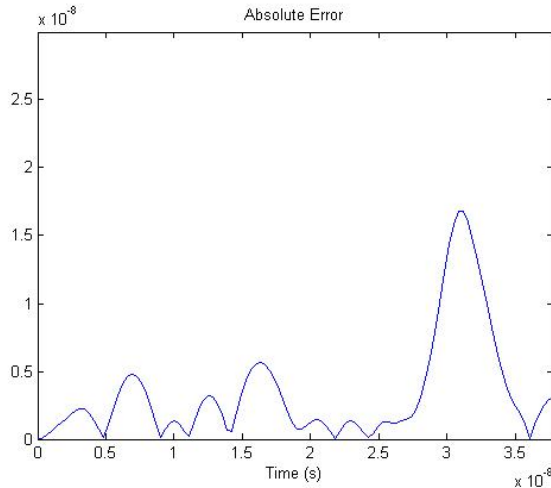


Figure 20: Modulus of absolute error between analytic and numerical solution of reflected electric field

Therefore from this analysis the absolute error of the peak of the wave from the analytical solution is $1.68 \times 10^{-8} \text{ Vm}^{-1}$, which equates to approximately 30% of the peak amplitude. Additionally the wavelength of the reflected wave has reduced by 0.2 m (6.7%) from the wavelength predicted from the theory.

6.2.2. Incident Angle = 45 Degrees

Using a similar analysis as above, we compare the analytical to numerical solution of the electric field at a distance 6.4 m from the dielectric, as shown in Figure 21: -

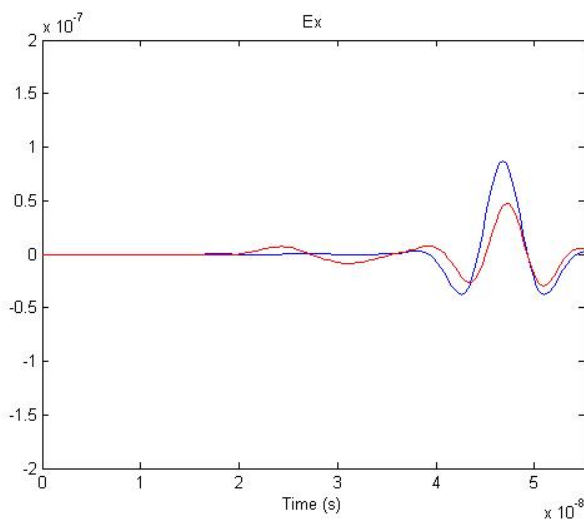


Figure 21: Analytic (blue) and numerical (red) solution for the electric field reflected off the dielectric

Again it is seen that the wavelength and amplitude of the wave is different for the analytic and numerical solution. The amplitude of the wave in the numerical solution is 44 % below that of the analytical solution. Performing a Fourier Transform (FFT) on the data, we can extract the frequencies that comprise the wave solutions: -

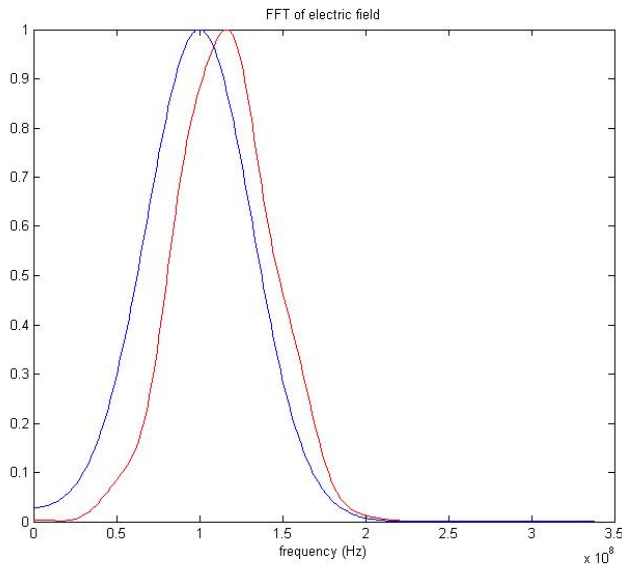


Figure 22: FFT of electric field numerical solution (red) against analytic solution (blue)

From Figure 22 we can see that the numerical solution has higher frequencies within the solution than the analytic solution predicts, with a peak at ~ 116 MHz (0.41 m reduction in wavelength) compared to the input frequency of 100 MHz. To examine this further we halve the grid spacing, Δy , to 0.1 m.

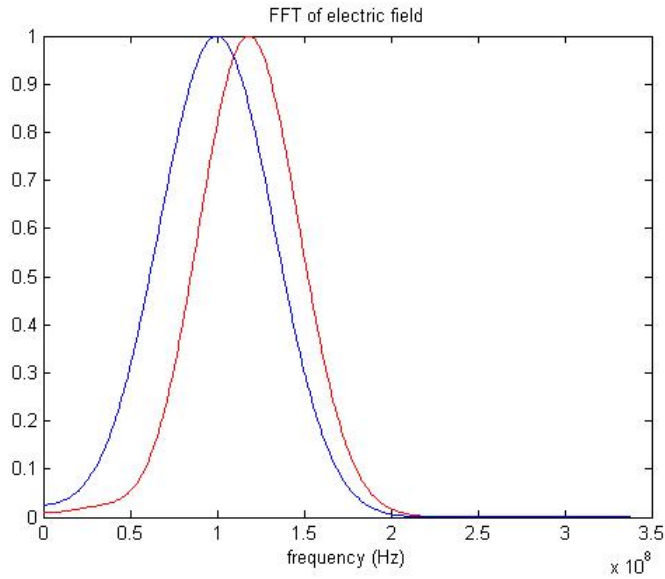


Figure 23: FFT of electric field numerical solution (red) against analytic solution (blue)

In this case there is a peak at the 118 MHz frequency, which equates to a reduction in wavelength of 0.45 m. Therefore reducing the grid spacing has not reduced the error in wavelength of the reflected wave, and therefore may suggest that some aspects of the numerical modelling appear not to be affected by the grid spacing.

6.3. Conclusions

From the free space and dielectric cases analysed here, the numerical solutions produce solutions which propagate in the correct directions compared to that predicted analytically; however a number of differences in behaviour are observed. In particular, the finite wave disperses tangentially away from the direction of propagation due to the Gaussian function used in truncating the electromagnetic wave to a finite radar pulse, as discussed previously. This results in a significant reduction in reflected amplitude of up to 44%, and this has serious consequences if attempting to produce RCS predictions using this method, as they are determined by considering the ratio of the reflected electric field amplitude to that of the incident field. There is also a reduction of wavelength in the numerical solution of up to 15 % compared to prediction, which has a consequence when determining the ability of a radar system to detect the reflected wave, as each radar will have a specific range of frequencies that it is sensitive to (given by its central frequency and its bandwidth).

Halving the grid spacing of the domain in the dielectric case did not reduce the error in the wavelength of the reflected wave. This may indicate that some aspects of the numerical method is unaffected by the change in grid spacing, as we expect the numerical solution to tend to the analytical solution as determined by the expression for the truncation error (see section 4.6.) The use of Gaussian functions to truncate the radar pulse spatially and radially may be responsible for this error. This requires further investigation to confirm or discount.

Possible approaches to remedy the effects of dispersion and change in wavelength of the radar pulse would be to examine the initial conditions and consider functions other than the Gaussian function to truncate the pulse. Additionally other numerical schemes such as the Lax-Wendroff approach investigated in [7] could have utility in modelling a radar pulse with sharp wavefronts.

7. Numerical Results from non-Time Harmonic Problem

The problem considered in this section is that of the radar signature of an object surrounded by plasma when interrogated by non-time harmonic electromagnetic waves. In particular this will examine the use of a chirped radar pulse to extract information regarding the plasma and object arrangement.

The use of chirp techniques by radar is an attempt to extract additional Doppler information from an observed target [14], and to reduce the vulnerability of the radar to jamming techniques such as chaff. The general arrangement to be considered is shown in Figure 24: -

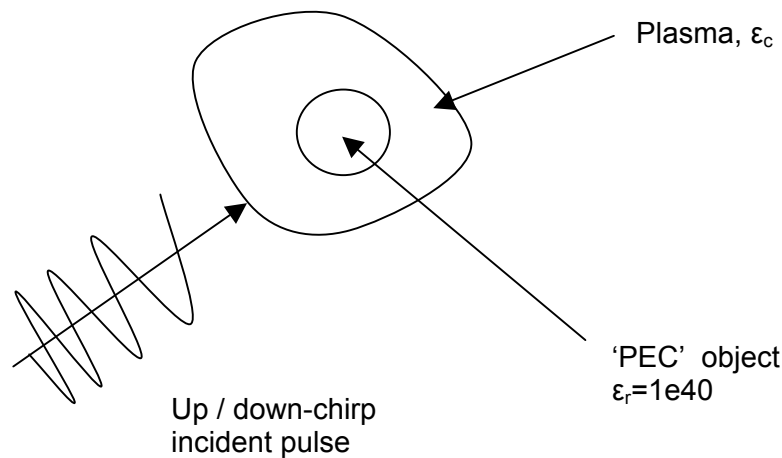


Figure 24: General arrangement of chirped pulse and plasma coated object

In this arrangement we have used the central frequency of the chirped pulse to determine the complex permittivity. The relative permittivity for the frequency extremes of the chirped pulse vary from this central value, as prescribed by equation (109). This approximation has been made due to the additional complexity of implementing a permittivity which will vary as the wavelength incident on that particular section of plasma changes. It is recognised that to determine the interaction of electromagnetic waves in plasma to a higher degree of fidelity, this approximation will need to be addressed in future work.

7.1 Incident Wave Representation

The radio wave will have the form of a radar pulse (as described in section 4.4. and utilised in section 6) which is Gaussian shaped both along and perpendicular to the Poynting vector of the electromagnetic fields in the pulse. For the purposes of this section, the wave is now taken to be non-time harmonic with an up-chirp (frequency increases linearly with time within the pulse see section 4.5.). The number of grid points used within the computational grid will be investigated and the effect on the solution (compared to expected behaviour) analysed. Initially a 150 MHz wave with an up-chirp of 250 MHz through the pulse length is considered.

7.2. Grid Spacing Variation

When performing numerical modelling of a sine wave, it is recommended in various texts, such as [1], that as an engineering standard, a minimum of 10 sampling points are required along a single wavelength in order to obtain a ‘good’ approximation. Using our condition (104) for minimum grid spacing for a dielectric material of relative permittivity ϵ_r , for the up-chirp wave that gives the recommended resolution of the wave at the 400 MHz ($\lambda = 0.75$ m) upper frequency limit the required grid spacing is: -

$$\Delta x = \Delta y = \Delta z = \min_{\underline{r} \in D} \left\{ \frac{\lambda_i}{10\sqrt{\epsilon_r(\underline{r})}} \right\} = \frac{0.075}{\sqrt{\epsilon_r}}. \quad (118)$$

By definition, the calculated relative permittivity in the plasma will be less than the free space permittivity ($\epsilon_r = 1$), so we determine the recommended minimum grid spacing to be 0.075 m. This equates to a sampling rate of the incident wave of 10 points per wavelength (highest frequency, $\lambda=0.75$ m) and severe over sampling of 26 points per wavelength for the lowest frequency in the chirp ($\lambda=2.0$ m).

To examine the effect of varying the sample rate of the wave on the error within the numerical solution, we examine the variation in wavelength of the transmitted pulse within the plasma. From the theory of electromagnetic waves propagating through a plasma (see section 5.) the wavelength of the wave will vary (specifically elongate), as it enters the plasma region. We will examine how the wavelengths predicted from the numerical solution compare to the wavelengths predicted from the theory for an up-chirped radar pulse. A schematic of the chirped incident wave is shown in Figure 25: -

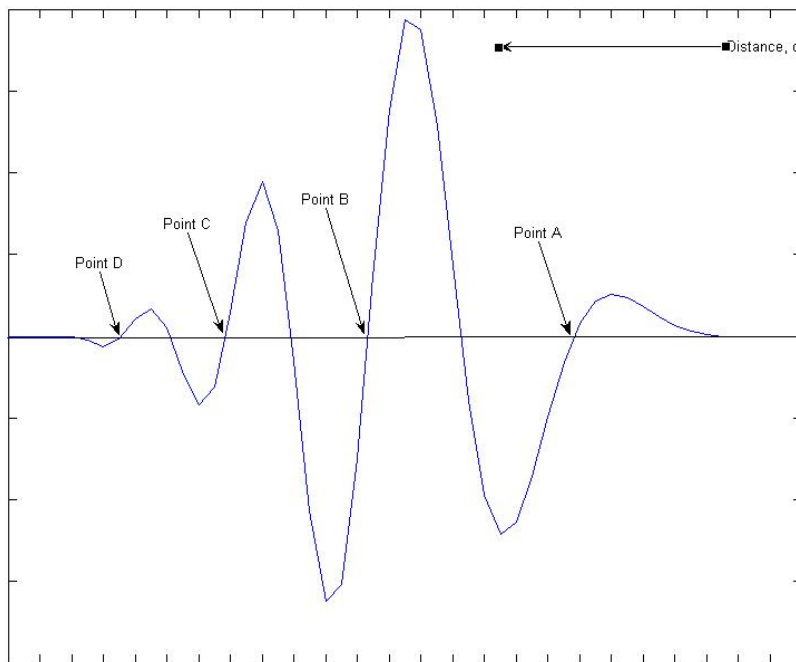


Figure 25: Schematic of the up-chirped incident wave

Examination of the incident wave shows that the points A, B, C and D are at 1.5 m, 3.55 m, 4.65 m and 5.6 m respectively. The pulse width is kept constant at 14.6 m, and the pulse length is 6.0 m. The time step, Δt , is constant in section of analysis, at 144.44 picoseconds (1.4444×10^{-10} s)

For this analysis, we will assume that the real part of the complex permittivity is constant in the plasma, taking the value 0.25. We also assume the plasma is cold

(the imaginary part of the complex permittivity is zero). As the relative permittivity is constant, we make the assumption that the plasma frequency will vary as the radar pulse passes into the plasma region. Therefore we determine the plasma frequency using: -

$$\begin{aligned}\varepsilon_r &= 1 - \frac{\omega_f^2}{\omega^2} \\ \Rightarrow \omega_f &= \omega \sqrt{1 - \varepsilon_r} \quad . \end{aligned} \tag{119}$$

Additionally, an expression for the wavelength of the transmitted wave (λ_f) can be produced based on the wavelength of the incident wave (λ) and relative permittivity:

$$\begin{aligned}\lambda_f &= \frac{2\pi c}{\sqrt{\omega^2 - \omega_f^2}} \\ \therefore \lambda_f &= \frac{2\pi c}{\sqrt{1 - \varepsilon_r} \omega} \\ \therefore \lambda_f &= \frac{\lambda}{\sqrt{1 - \varepsilon_r}} \quad . \end{aligned} \tag{120}$$

Given our choice of relative permittivity, in this case $(1 - \varepsilon_r)^{1/2}$ equals 0.5, the wavelength of the wave in the plasma is twice that in free space (the incident wavelength), i.e. $\lambda_f = 2\lambda$. Table 1 details the four points of the incident wave to be considered for the numerical analysis: -

	Point A	Point B	Point C	Point D
Distance along pulse, d (m)	1.5	3.55	4.65	5.6
Wavelength, λ (m)	2.04	1.56	1.08	0.84
Frequency, f (MHz)	147.06	192.31	277.78	357.14
Plasma frequency, f_f (MHz)	127.36	166.55	240.56	309.29
Wavelength in plasma, λ_p (m)	4.08	3.12	2.16	1.68

Table 1: Details of up-chirped pulse incident on cold plasma plane

The grid spacing is varied such that the lowest plasma wavelength in the chirped pulse is sampled between 10 and 3 grid points, with a single grid point removed

per iteration. The numerical solution is examined to determine the wavelength of the pulse at points A, B, C and D, and these are compared to those wavelengths predicted from theory. Table 2 shows the results of this analysis: -

Number of sample points at $\lambda_p = 1.5$ m	Grid spacing $\Delta x = \Delta y = \Delta z$ (m)	Wavelength from numerical solution at Point A	Wavelength from numerical solution at Point B	Wavelength from numerical solution at Point C	Wavelength from numerical solution at Point D
10	0.15000	4.20	3.20	2.50	2.00
9	0.16667	4.25	3.33	2.50	2.00
8	0.18750	4.31	3.38	2.53	2.06
7	0.21429	4.18	3.43	2.68	2.25
6	0.25000	4.50	3.50	2.75	2.25
5	0.30000	4.50	3.60	3.00	2.40
4	0.37500	4.50	3.94	3.38	3.00
3	0.50000	5.00	4.25	3.50	3.50

Table 2: Recorded wavelengths of numerical solution of wave travelling in plasma

These results are plotted in Figure 26: -

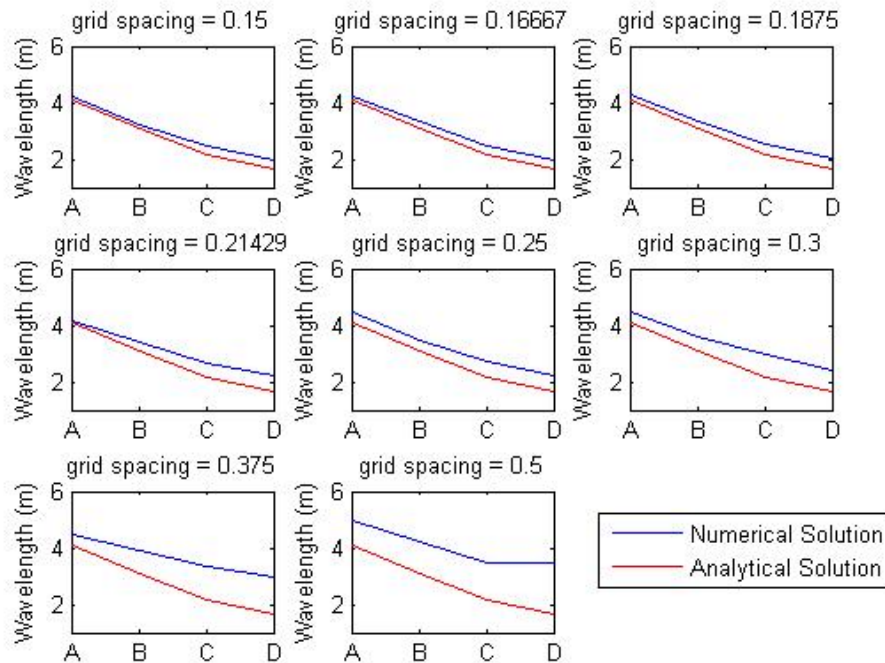


Figure 26: Comparison of wavelengths of chirped pulse extracted from numerical solution to analytical values

These results show a consistent variation of the wavelength in the chirp derived from the numerical solution to the theory at point D (i.e. the high frequency, low

wavelength end of the chirp). The slope of the chirp predicted by the numerical solution is consistent with the theory for grid spacing 0.15 to 0.3 m, and it can be seen that when the grid spacing equals 0.375 m, the chirp begins to lose its shape (the gradient of the wavelength varies from the incident wave).

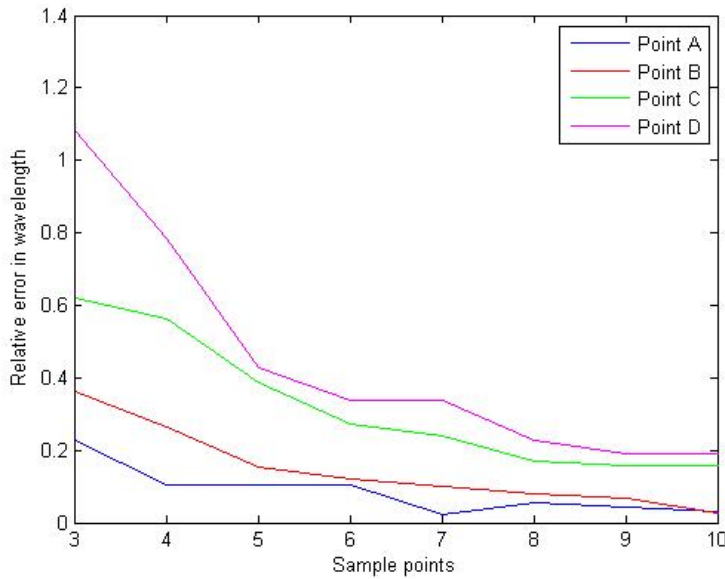


Figure 27: Relative error in wavelength of transmitted wave as grid spacing (and therefore incident wave sampling rate) is varied.

Figure 27 shows that the error in wavelength from the numerical solution increases as the number of points sampling the wave is reduced. Of particular interest is the fact that these four lines are not parallel, that is the error in the chirped wave for the low wavelengths increases as the number of sampling points decreases. This would suggest that there may be some effect by reducing the sampling rate of the wave on the overall error of the solution. However, this must be investigated further as this initial approach involved decreasing the grid spacing for the whole grid, and by the expression for the truncation error (see section 4.6.) we expect the error in the solution to reduce by Δy^2 .

7.3. Variation of Chirp in Incident Wave

We now consider an incident wave on a plane of plasma (with fixed electric permittivity of 0.25) with a significant amount of chirp to see the error in the numerical solution throughout the wave as time progresses. By keeping the grid spacing fixed the sampling rate of the wave will vary along the incident pulse and allow analysis of the error as a function of sampling rate.

A down-chirped wave, from 550 MHz to 200 MHz, is allowed to propagate into the region of the computational domain modelled as cold plasma. After 150 time steps ($\Delta t = 1.4444 \times 10^{-10}$ s), the numerical solution for the wave in the plasma is shown in Figure 28. In this figure a wave corresponding to the incident wave with doubled wavelength is shown for comparison.

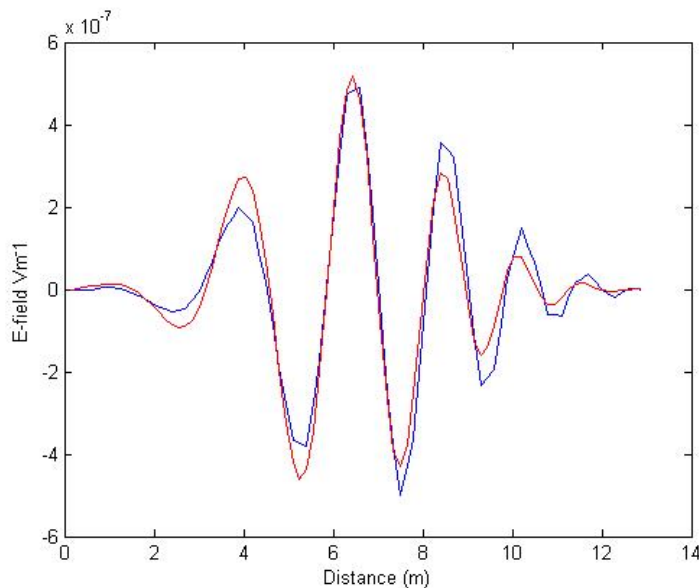


Figure 28: Comparison of numerical solution of wave in plasma (red line) against incident wave (blue line) with doubled wavelength

From this figure it can be seen that the right hand side (high frequency) of the region that the numerical solution for the wave has an amplitude that is lower than the incident wave, while the numerical solution for the low frequency end shows the opposite effect. This is due to the effect of the group velocity of the

wave in the plasma, with the 'information' (the Gaussian modulation of the wave in the direction of propagation) propagating at a slower velocity than the phase of the wave.

The phase velocity of the wave in the plasma is given by equation (111), and can be combined with the expression for the wave number and plasma frequency of the wave.

$$\begin{aligned}
 v_p^2 &= c^2 + \frac{\omega_p^2}{k^2} \\
 k^2 &= \frac{\epsilon_r \omega^2}{c^2} \\
 \therefore v_p^2 &= c^2 + \frac{c^2 \omega_p^2}{\epsilon_r \omega^2} \quad . \quad (121)
 \end{aligned}$$

Using equation (120), this further simplifies to: -

$$\begin{aligned}
 v_p^2 &= c^2 + \frac{c^2(1-\epsilon_r)\omega^2}{\epsilon_r \omega^2} \\
 \Rightarrow v_p^2 &= c^2 + \frac{c^2(1-\epsilon_r)}{\epsilon_r} \\
 \Rightarrow v_p &= \frac{c}{\sqrt{\epsilon_r}} \quad . \quad (122)
 \end{aligned}$$

For our electric permittivity of 0.25, this implies that the phase velocity will be 2c, i.e. twice the speed of light in vacuum. The group velocity is given by equation (112) and gives a value of 0.5c.

The phase velocity for the down-chirped wave was extracted by examining the position of the peaks in the wave relative to the y-axis at time 2.0216×10^{-8} seconds and 2.3104×10^{-8} seconds, as shown in Table 3: -

Peak Number	Wavelength (m)	Distance (m), $t=2.0216 \times 10^{-8}$ s	Distance (m), $t=2.3104 \times 10^{-8}$ s	Phase Velocity (multiples of c)	Error in phase velocity (multiples of c)
1	0.6389	10.575	12.3	1.9910	-0.0090
2	0.687	9.925	11.65	1.9910	-0.0090
3	0.7909	9.175	10.9	1.9910	-0.0090
4	0.8449	8.4	10.15	2.0199	0.0199
5	0.9469	7.5	9.275	2.0487	0.0487
6	1.044	6.55	8.275	1.9910	-0.0090
7	1.18	5.475	7.2	1.9910	-0.0090
8	1.319	4.3	6.075	2.0487	0.0487
9	1.505	3.025	4.775	2.0199	0.0199
10	1.741	1.6	3.4	2.0776	0.0776

Table 3: Examination of phase velocities recorded from numerical solution of the electromagnetic wave in the plasma

The phase velocities recorded from the numerical solution have a mean of 2.0170c, with a standard deviation 0.0318c. The phase velocities for the low wavelengths tend to be lower than predicted, and for the higher wavelengths are greater than predicted. Figure 29 summarizes these findings in terms of the sampling rate of the incident wave and the relative error in phase velocity: -

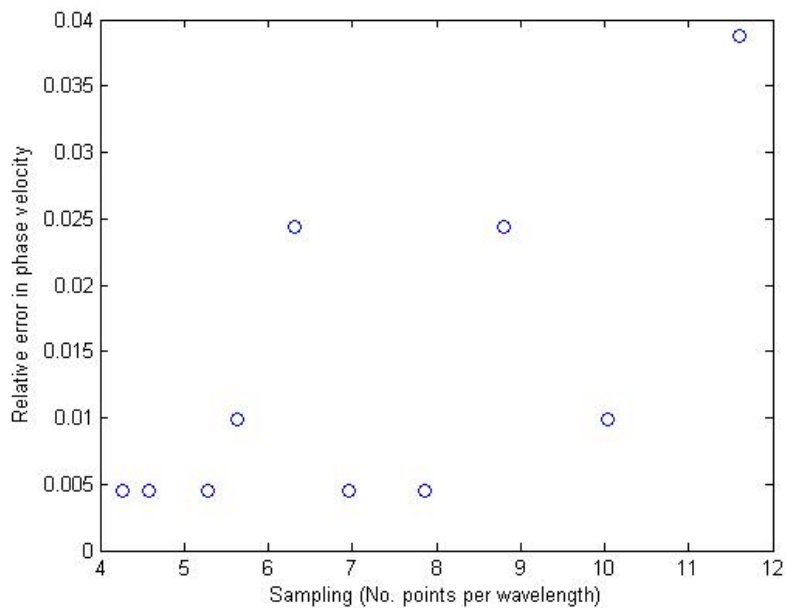


Figure 29: Relative error in phase velocity of numerical solution

There appears to be some increase in error of phase velocity as the number of sampling points of the incident wave increases to 11.6 points per wavelength. The numerical solution for the other points is within 2.5% of the actual phase velocity predicted by theory; this is discussed further in 7.4. The wavelengths within the chirped pulse were extracted by examining the difference in distance along the y-axis of adjacent peaks in the numerical solution, as shown in Figure 30: -

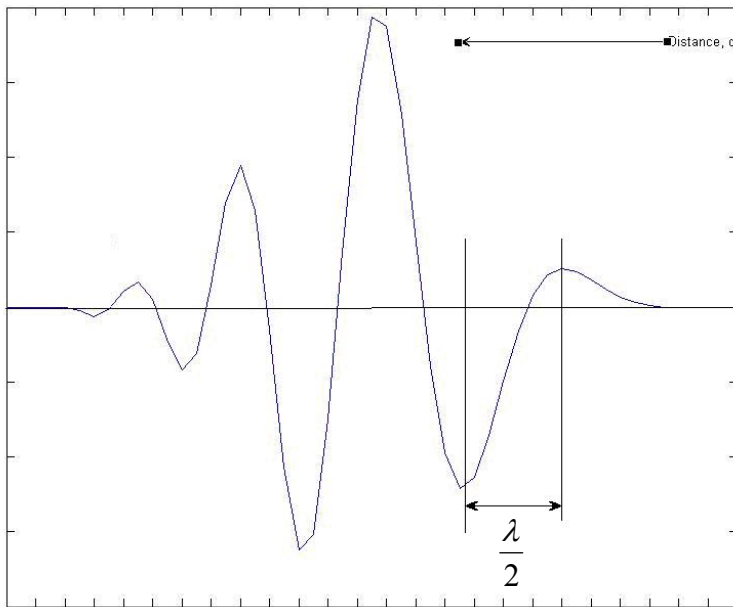


Figure 30: Schematic of wavelength measurement

A comparison of the wavelengths of the analytic solution to the numerical solution is shown in Figure 31: -

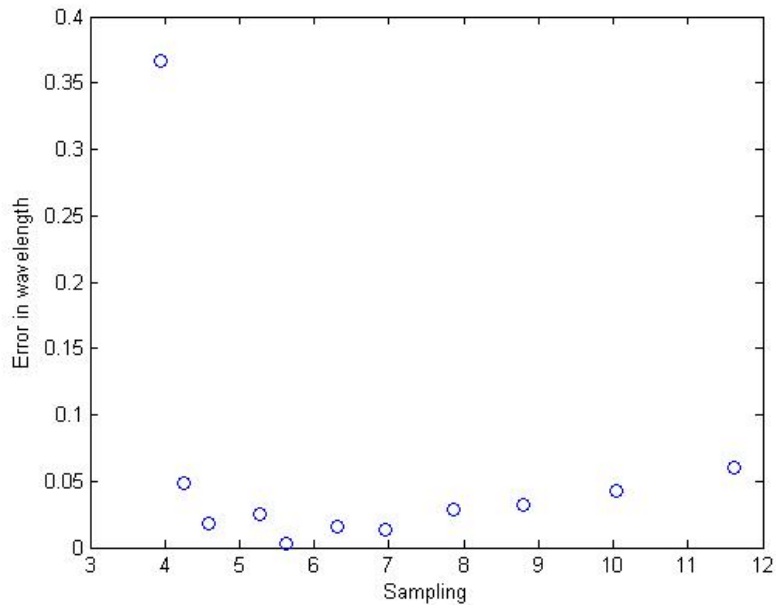


Figure 31: Relative error in wavelength (in meters) against sampling rate of incident wave (points per wavelength)

From Figure 31 it can be seen that for the chirped wave regions sampled at greater than 4 points per wavelength, the wavelength from the numerical solution is within 5 % of that predicted analytically. Below this sampling rate, the numerical solution shows significant deviation from theory reporting a wavelength with a relative error of 37%. In general there is also an increase in relative error as the number of sampling points increases up to the maximum sample rate. There are two possibilities for this behaviour, either the methodology used to obtain the wavelength is flawed, or this is an effect caused by the use of the Gaussian function along the wave. Further investigation is required to determine this.

From this analysis, the requirement to sample a sinusoidal wave by ten points per wavelength appears to be invalid, as there appears to be no loss of phase information of the wave for a sampling rate of 4 points per wavelength, which appears to be the lower limit for sampling.

7.4. Conclusions

From the analysis in this section, it is concluded that the use of a Yee grid and finite radar pulse has utility in accurately modelling the behaviour of chirped electromagnetic waves in plasma. The minimum number of sampling points required to use this approach is assessed to be 4 points per wavelength at the high frequency end of the chirp. Numerical results in this region for the wavelength and phase velocity of the wave propagating in the plasma are within 5 % and 4 % of the analytical solution respectively. No examination of the group velocity has been made in this analysis, and is left as an area for future research.

8. Summary

The research within this report has shown that the FDTD has the utility to model the propagation of electromagnetic waves in various media. When modelling finite radar pulses rather than infinite, time-harmonic incident fields, careful consideration must be given to the shape and composition of the numerical grid and initial conditions, in particular to reduce the dispersion of the pulse perpendicular to the direction of motion. In this report a Gaussian function has been utilised to set up a continuous, and differentially continuous, incident pulse; which may be up or down chirped.

Numerical results for a time harmonic wave propagating in free space show a reduction in the peak amplitude of the electric field of up to 0.5% per time step, although this rate is reduced by 35% when the pulse width was doubled.

Analysis of the numerical solutions from the examples considered has shown the method used in this report can predict electric field peak amplitudes (as predicted by Snell's law/Fresnel equations) of a reflected wave off a dielectric surface to within approximately 60% percent. This accuracy is dependent on the angle of incident on the wave, grid spacing chosen and dimensions of the pulse as defined in the examples in section 6. Due to the size of this error, this method is not recommended for use in determining RCS values of dielectrics, due to the requirement to accurately determine reflected electric field amplitudes.

Additionally a systematic error in the wavelength of the radio wave reflected off a dielectric was observed, which may be due to the use of a Gaussian function along the length of the pulse, though further research is required to confirm this.

An investigation into the required resolution of the modelled chirped radar pulse (incident on a plasma) to produce numerical results which are consistent with electromagnetic theory has shown that a sampling rate of four points per wavelength appears to be sufficient to ensure the phase information and phase velocity of the transmitted pulse is recoverable from the numerical solution. From

the results there appears to be some increase in error of the plasma wavelength as the number of sampling points increases. It is postulated that this is due either to the use of a Gaussian function in the pulse or due to an error induced in the methodology of measuring the wavelength in the solution.

The use of a Gaussian function to truncate an infinite sine wave so that a finite radar pulse in space can be represented numerically appears to be problematic. The analysis in this report has shown that the numerical solution for a finite pulse propagating in a dielectric/plasma exhibits dispersion as the computation progresses forward in time. Dispersion of the electric field is observed tangentially to the direction of propagation of the wave.

Future work in this area would be to investigate different finite difference formulations of Maxwell's equations, and assess their capability to model non-time harmonic radio waves. An extension of this work would be to determine other methods of representing a finite radar pulse within the computational domain, so that the dispersion of the Gaussian function observed in this work may be negated, for example the Lax-Wendroff approach investigated in [7] is reported to have good utility in modelling sharp wavefronts. Additionally it is recommended that adaptive, moving meshes be investigated to assess their capability in modelling a chirped radio wave, as this would allow a constant sampling rate along the whole length of the incident radar pulse, which should result in the error in the numerical solution being equally distributed throughout the whole volume of the pulse. Finally, the ability of a radar system to extract information from the chirped pulse reflected off a plasma coated object should be investigated further.

9. References

1. The Finite Difference Time Domain Method for Electromagnetics, K. S. Kunz and R. J. Luebbers, 1993.
2. Introduction to Plasma Physics, F. F. Chen, 1974.
3. Basic Electromagnetism, E. R. Dobbs, 1993.
4. Radar Cross Section handbook, Volume 2, Ruck et al, 1970.
5. Introduction to Radar Systems, Third Edition, M. I. Skolnik, 2001.
6. Relative Accuracy of Several Finite-Difference Time-Domain Methods in Two and Three Dimensions. K. L. Shalager et al, IEEE, Vol. 41, No. 12 (1993) pg 1732 – 1737.
7. A New Finite-Difference Time-Domain Algorithm for the Accurate Modelling of Wide-Band Electromagnetic Phenomena, S. R. Omick, S. P. Castillo, IEEE, Vol. 35, No. 2 (1993) pg 215 – 222.
8. Numerical research on the RCS of plasma, Z. Yu et al, IEEE, (2003) pg 428 – 432.
9. Three-Dimensional Computation of Reduction in Radar Cross Section Using Plasma Shielding, B. Chaudhury, S. Chaturvedi, IEEE, Vol. 33, No. 6, (2005), pg 2027 – 2034.
10. The Calculation of Back-Scattering Radar cross Section of Plasma Spheres, Y. Gao et al., 25th International Conference on Infrared and Millimeter Waves, 2000, pg 415 – 416.
11. Absorbing Boundary Conditions for the Finite-Difference Approximation of the Time-Domain for Electromagnetic-Field Equations, G. Mur, IEEE, Vol. EMC-23, No. 4, (1981), pg 377 – 382.
12. Ionospheric Radio, K. Davies, 1990.
13. Numerical Solution of Initial Value Problems involving Maxwell's Equation in Isotropic Media, K. S. Yee, IEEE, Vol. 14, (1966), pg 302.
14. Modern Radar Systems, H. Meikle, 2001.

Appendix A: Vector identities

Lemma 1

$$\nabla \cdot \nabla \times \underline{A} = 0$$

Proof

$$\begin{aligned}\nabla \times \underline{A} &= \begin{vmatrix} \underline{i} & \underline{j} & \underline{k} \\ \frac{\partial}{\partial x} & \frac{\partial}{\partial y} & \frac{\partial}{\partial z} \\ A_x & A_y & A_z \end{vmatrix} = \\ & \underline{i} \left(\frac{\partial A_z}{\partial y} - \frac{\partial A_y}{\partial z} \right) + \underline{j} \left(\frac{\partial A_x}{\partial z} - \frac{\partial A_z}{\partial x} \right) + \underline{k} \left(\frac{\partial A_y}{\partial x} - \frac{\partial A_x}{\partial y} \right) = \underline{B} \quad , \\ \nabla \cdot \underline{B} &= \frac{\partial B_x}{\partial x} + \frac{\partial B_y}{\partial y} + \frac{\partial B_z}{\partial z} \\ \nabla \cdot \nabla \times \underline{A} &= \frac{\partial}{\partial x} \left(\frac{\partial A_z}{\partial y} - \frac{\partial A_y}{\partial z} \right) + \frac{\partial}{\partial y} \left(\frac{\partial A_x}{\partial z} - \frac{\partial A_z}{\partial x} \right) + \frac{\partial}{\partial z} \left(\frac{\partial A_y}{\partial x} - \frac{\partial A_x}{\partial y} \right) \\ &= \frac{\partial^2 A_z}{\partial x \partial y} - \frac{\partial^2 A_y}{\partial x \partial z} + \frac{\partial^2 A_x}{\partial y \partial z} - \frac{\partial^2 A_z}{\partial y \partial x} + \frac{\partial^2 A_y}{\partial z \partial x} - \frac{\partial^2 A_x}{\partial z \partial y} \quad , \end{aligned}$$

for sufficiently well behaved vector field (i.e. with no discontinuities) the order of partial differentiation is unimportant, i.e.:-

$$\frac{\partial}{\partial x} \left(\frac{\partial B}{\partial y} \right) = \frac{\partial}{\partial y} \left(\frac{\partial B}{\partial x} \right) ,$$

and so on for each Cartesian co-ordinate differential combination, so that we achieve the result: -

$$\nabla \cdot \nabla \times \underline{A} = 0$$

■

Lemma 2

$$\nabla \times (\nabla \times \underline{A}) = -\nabla^2 \underline{A} + \nabla(\nabla \cdot \underline{A})$$

Proof

$$\begin{aligned} \nabla \times (\nabla \times \underline{A}) &= i \left(\frac{\partial^2 A_y}{\partial y \partial x} - \frac{\partial^2 A_x}{\partial y^2} + \frac{\partial^2 A_z}{\partial z \partial x} - \frac{\partial^2 A_x}{\partial z^2} \right) + j \left(\frac{\partial^2 A_x}{\partial y \partial x} - \frac{\partial^2 A_y}{\partial x^2} + \frac{\partial^2 A_z}{\partial z \partial y} - \frac{\partial^2 A_y}{\partial z^2} \right) \\ &\quad + k \left(\frac{\partial^2 A_x}{\partial z \partial x} - \frac{\partial^2 A_z}{\partial x^2} + \frac{\partial^2 A_y}{\partial z \partial y} - \frac{\partial^2 A_z}{\partial y^2} \right) \\ &= i \left(-\frac{\partial^2 A_x}{\partial y^2} - \frac{\partial^2 A_x}{\partial z^2} \right) + j \left(-\frac{\partial^2 A_y}{\partial x^2} - \frac{\partial^2 A_y}{\partial z^2} \right) \\ &\quad + k \left(-\frac{\partial^2 A_z}{\partial x^2} + -\frac{\partial^2 A_z}{\partial y^2} \right) + i \left(\frac{\partial^2 A_y}{\partial y \partial x} + \frac{\partial^2 A_z}{\partial z \partial x} \right) + j \left(\frac{\partial^2 A_x}{\partial y \partial x} + \frac{\partial^2 A_z}{\partial z \partial y} \right) \\ &\quad + k \left(\frac{\partial^2 A_x}{\partial z \partial x} + \frac{\partial^2 A_y}{\partial z \partial y} \right) \\ &= i \left(-\frac{\partial^2 A_x}{\partial y^2} - \frac{\partial^2 A_x}{\partial z^2} \right) + j \left(-\frac{\partial^2 A_y}{\partial x^2} - \frac{\partial^2 A_y}{\partial z^2} \right) \\ &\quad + k \left(-\frac{\partial^2 A_z}{\partial x^2} + -\frac{\partial^2 A_z}{\partial y^2} \right) + i \left(\frac{\partial^2 A_y}{\partial y \partial x} + \frac{\partial^2 A_z}{\partial z \partial x} \right) + j \left(\frac{\partial^2 A_x}{\partial y \partial x} + \frac{\partial^2 A_z}{\partial z \partial y} \right) \\ &\quad + k \left(\frac{\partial^2 A_x}{\partial z \partial x} + \frac{\partial^2 A_y}{\partial z \partial y} \right) + i \left(\frac{\partial^2 A_x}{\partial x^2} - \frac{\partial^2 A_x}{\partial x^2} \right) + j \left(\frac{\partial^2 A_y}{\partial y^2} - \frac{\partial^2 A_y}{\partial y^2} \right) \\ &\quad + k \left(\frac{\partial^2 A_z}{\partial z^2} - \frac{\partial^2 A_z}{\partial z^2} \right) \\ &= i \left(-\frac{\partial^2 A_x}{\partial x^2} - \frac{\partial^2 A_x}{\partial y^2} - \frac{\partial^2 A_x}{\partial z^2} \right) + j \left(-\frac{\partial^2 A_y}{\partial x^2} - \frac{\partial^2 A_y}{\partial y^2} - \frac{\partial^2 A_y}{\partial z^2} \right) \\ &\quad + k \left(-\frac{\partial^2 A_z}{\partial x^2} - \frac{\partial^2 A_z}{\partial y^2} - \frac{\partial^2 A_z}{\partial z^2} \right) + i \frac{\partial}{\partial x} \left(\frac{\partial A_x}{\partial x} + \frac{\partial A_y}{\partial y} + \frac{\partial A_z}{\partial z} \right) + j \frac{\partial}{\partial y} \left(\frac{\partial A_x}{\partial x} + \frac{\partial A_y}{\partial y} + \frac{\partial A_z}{\partial z} \right) \\ &\quad + k \frac{\partial}{\partial z} \left(\frac{\partial A_x}{\partial x} + \frac{\partial A_y}{\partial y} + \frac{\partial A_z}{\partial z} \right) \\ &= -\nabla^2 \underline{A} + \nabla(\nabla \cdot \underline{A}) \end{aligned}$$

■